The dynamics of predissociating high Rydberg states of NO

M. Bixon and Joshua Jortner
School of Chemistry, Tel Aviv University, 69978, Tel Aviv, Israel

(Received 29 January 1996; accepted 28 March 1996)

In this paper we present a theoretical study of the predissociation dynamics of the $nf(N^+=2)$ (with the principal quantum numbers $n=40-95$) and the $np(N^+=0)$ ($n=70-125$) Rydberg series of NO, which exhibit a marked lifetime dilution (lengthening) at $n>65$ for the f series and at $n>116$ for the p series [M.J.J. Vrakking and Y. T. Lee, J. Chem. Phys. **102**, 8818 (1995)]. The multichannel effective Hamiltonian with several doorway (for excitation) and escape (for decay) states was constructed using experimental information on the quantum defects and on the decay width constants incorporating both intramolecular coupling and exterior electric field coupling between high Rydbergs. The analysis of the intramolecular Rydberg electron–core dipole long range coupling ($H_{\text{R-D}}$) in conjunction with the energy gaps between proximal pairs of energy levels, which are subjected to appropriate selection rules, reveals that (i) for low $l(\leqslant 3)$ core-penetrating Rydbergs only a small number of accidental near-resonances are exhibited, and (ii) for high $l(>3)$ nonpenetrating Rydbergs the electron-core dipole coupling decreases fast with increasing l, i.e., $(H_{\text{R-D}})\propto l^{-7}$. The general characteristics of the high $l(>3)$ manifold establish a bottleneck effect, which precludes intramolecular l mixing, implying that high Rydberg lifetime dilution effects can be induced only by exterior electric field coupling (H_{STARK}). Parameter-free multichannel effective Hamiltonian calculations were conducted under narrow-band excitation conditions, which interrogate the electric field induced mixing in the energetic vicinity of the doorway state. The electric field induced l mixing model accounts semiquantitatively for the electric field dependence of the energy-resolved line shapes of the $nf(N^+=2)$ series and for the n and electric field dependence of the lifetimes of the $nf(N^+=2)$ and the $np(N^+=0)$ series. Accidental near-resonant simultaneous intramolecular and electric field coupling $np(N^+=0) \overset{H_{\text{R-D}}}{\leftrightarrow} n'd(N^+=1) \overset{H_{\text{STARK}}}{\leftrightarrow} n'l(\geqslant 3)(N^+=1)$ for two sets of proximal states $n=92$, $n'=80$ and $n=95$, $n'=82$, result in mediated-sequential mixing, which is manifested by slow decay times below the onset of effective electric field mixing by weak ($F_0\simeq 0.04-0.08$ V/cm) stray electric fields. © *1996 American Institute of Physics.* [S0021-9606(96)02125-3]

I. A PROLOGUE ON THE DYNAMICS OF HIGH RYDBERG STATES

The dynamics of high Rydberg states ($n\simeq 10-250$, where n is the principal quantum number) of atoms, diatomic molecules, large molecules, and clusters,[1–14] which was explored by zero electron kinetic energy (ZEKE) spectroscopy[1–9,12–14] and by related pulsed field ionization[10,11] (PFI) methods, constitutes a significant extension of the broad and interesting research area of atomic[15,16] and intramolecular[17–27] radiationless transitions. The radiationless transitions of high Rydbergs can be envisioned as relaxation in microsystems (mean radius $\langle r\rangle=(3/2)n^2\ a_0$, e.g., $\langle r\rangle=1\ \mu$m for $n=112$), which is subjected to strict propensity rules, i.e., occurring from core-penetrating low electron angular momentum l states in the spatial region close to the nucleus (range A in Fano's terminology[28,29]). The radiationless transitions of high n, low l Rydbergs involve atomic autoionization,[12,13,15,16,30] and ''reactive'' intramolecular dynamics,[28,29,31–40] i.e., molecular predissociation[10,11,37] and/or autoionization[8,14,31–37] and intramolecular ''nonreactive'' dynamics in a bound level structure, i.e., internal conversion.[9,38,39] The partial widths $\Gamma^I_{lJ\alpha}(n)$ for the decay of a given $|nlJ\alpha\rangle$ Rydberg (where J is the total angular momentum and α labels other quantum numbers) with a quantum defect $\delta(l\alpha)$ into all the open radiationless channels (I) are expected to be determined by the n^3 scaling law.[9,10,13,30–40] The total decay width

$$\Gamma_{lJ\alpha}(n)=\sum_I \Gamma^I_{lJ\alpha}(n) \tag{1.1}$$

of the $|nlJl\alpha\rangle$ Rydberg is

$$\Gamma_{lJ\alpha}(n)=\Gamma_0(lJ\alpha)/\nu^3, \tag{1.2}$$

where the effective quantum number is $\nu=[n-\delta(l\alpha)]$ and $\Gamma_0(lJ\alpha)$ is the decay constant. The n^3 scaling law applies well for the radiationless decay of moderately high Rydbergs of atoms,[12,13,41–43] diatomics[10,11,37] and large molecules,[9] inferred from Lorentzian (or Fano-type) spectral line broadening[9,12,13,37,41–43] or from time-resolved ion counting PFI spectroscopy.[10] In this n region $\Gamma(n)=\Gamma_0/n^\alpha$ with α being close to 3.0 (Table I). At higher values of n, the breakdown of the n^3 scaling law, Eq. (1.2) is exhibited, as interrogated by time-resolved ZEKE spectroscopy[1–9,12–14] and by time-resolved ion counting PFI spectroscopy.[10] This interesting effect was originally observed for the np Rydberg series of NO,[3] and subsequently documented for the np and nf series of NO,[10] for the Rydbergs of large molecules[8] and for

TABLE I. Universality of the dynamics of high Rydbergs of atoms, diatomics and large molecules.

System	Decay channel(s)	δ	α	"Low" n[a] Γ_0 (cm^{-1})	"High" n[a] n_M (a)	$D(n_M)$ (b)	$n_M^{(1)}$ ($F=0.05$ V/cm) (c)	$\gamma\rho(n_M^{(1)})$ (d)
Ar nd' (e)	Autoionization	0.18	⋯	31 000	70–75	100 ($n=80$)	104	0.39
Ar np' (f)	Autoionization	1.68	3.0 ± 0.1	2100	$\geqslant 100$	100 ($n=120$)	116	1.5×10^{-2}
NO $nf(N^+=2)$ (g)	Predissociation	0.01	3.0 ± 0.1	43	65	15 ($n=65$)	58	9.8×10^{-3}
NO $np(N^+=0)$ (g)	Predissociation	0.728	3.0 ± 0.1	1610	116	50 ($n=120$)	113	1.3×10^{-2}
BBC (h)	Internal conversion	1.38	2.5 ± 0.5	8000	>25 <100	300 ($n=100$)	120	5.7×10^{-2}
DABCO (h)	Internal conversion & autoionization	0.41	2.5 ± 0.5	6400	>45 <55	1000 ($n=100$)	122	4.2×10^{-2}

[a]"Low" n is characterized by $n<n_M$, while "high" n is characterized by $n>n_M$. The value of n_M in each case is obtained under the specific experimental conditions.
[b]Experimental dilution factor at the specified value of $n\geqslant n_M$ (given in parentheses).
[c]$n_M^{(1)}$ represents the calculated value of n for $F=1$ (the onset of strong mixing) and $F=0.05$ V/cm.
[d]Calculated from Eq. (1.5).
[e]Reference 12.
[f]Reference 13.
[g]Reference 10.
[h]Reference 9.

the nd' (Ref. 12) and the np' (Ref. 13) autoionizing states of Ar. At $n>n_M$ (where the threshold value of n, which is denoted by n_M, depends on the specific experimental conditions) one encounters a dramatic lengthening of the lifetimes $\tau(n)=\hbar/\Gamma(n)$. The lifetime lengthening is expressed by the dilution factor[9,10,12,13,38–40,44–47]

$$D(n)\simeq\tau(n)/(n^3\hbar/\Gamma_0). \tag{1.3}$$

The available experimental data summarized in Table I demonstrate the universality of the lifetime lengthening effect of high Rydbergs for autoionization in atoms, for autoionization and predissociation in diatomics, and for internal conversion and autoionization in large molecules.

The conceptual framework for the dynamics of high Rydbergs was provided by the electric field-induced coupling and mixing model advanced, developed, and utilized by Bordas *et al.*[44] Chupka,[45,46] Merkt, and Zare,[47] Jortner and Bixon[38–40] and Vrakking and Lee.[10] We pursued[38–40] the formal analogy between the coupling, accessibility, and decay of high Rydbergs in external weak electric fields (field strength $F=0.01-1$ V/cm) and intramolecular (nonadiabatic or/and spin–orbit) coupling, excitation, and relaxation in a bound level structure of an isolated molecule. General considerations result in two semiquantiative results, which provide insight into

(a) The onset of strong mixing.[10,38–40] The effective field-induced mixing of an nl Rydberg [with a quantum defect $\delta(l)$] with the inactive high l' ($l'>3$) manifold is specified in terms of the homogeneous electric field, which is expressed in reduced units[38–40]

$$\overline{F}(n,l)=(F/\mathrm{V\ cm^{-1}})n^5/3.4\times10^9[\,\delta(l)\mathrm{mod}(1)]. \tag{1.4}$$

The onset of mixing[39,40] is realized for $\overline{F}(nl)\gtrsim 0.5-1.0$, while strong mixing prevails[39,40] when $\overline{F}(n,l)>1-3$. In Table I we have provided the values of $n=n_M^{(1)}$, which correspond to $F=1$ at $F=0.05$ V/cm, representing a typical stray electric field in a ZEKE apparatus, or in a time-resolved ion counting PFI experimental setup. Equation (1.4) indicates that the onset of the dilution of lifetimes is given by $n_M=80.6\eta[\,\delta(l)(\mathrm{mod}1)]^{1/5}(F/\mathrm{V\ cm^{-1}})^{-1/5}$, being determined by the quantum defect and the electric field, where η is a numerical factor in the region $\eta=1$ (for $\overline{F}=1$) and $\eta=1.25$ (for $\overline{F}=3$).

(b) The level structure of the mixed states.[38] At the onset of strong mixing, i.e., for $n>n_M$ (at a given value of F) the product $\gamma\rho(n_M)$ of the average decay widths γ of the mixed molecular eigenstates by their density of states $\rho(n_M)$ is[38]

$$\gamma\rho(n_M)=\Gamma_0/4\ \mathrm{Ry}[\delta(l)\,\mathrm{mod}(1)] \quad n=n_M, \tag{1.5}$$

where Ry is the Rydberg constant. $\gamma\rho(n_M)$ is independent of n_M and of F. With increasing n ($\geqslant n_M$) the parameter $\gamma\rho(n)$ is $\gamma\rho(n)=\gamma\rho(n_M)\ (n_M/n)^5$, decreasing with increasing

energy.[38] From the $\gamma\rho(n_M)$ data (Table I) calculated from Eq. (1.5) we conclude that for all the high Rydberg systems studied up to date $\gamma\rho(n_M)\ll 1$ and also $\gamma\rho(n>n_M)\ll 1$. Accordingly, the mixed level structure corresponds to the sparse limit of isolated resonances.

These heuristic arguments, which rest on a single channel picture, have to be extended and supplemented by detailed multichannel calculations. The effective Hamiltonian formalism[19,22–25] was advanced and utilized[38–40] to treat the dynamics of high Rydbergs in weak electric fields. The theoretical treatment utilizes as input data quantum defects $\delta(l\alpha)$, which are obtained from spectroscopy and decay width constants $\Gamma_0(l\alpha)$, which are extracted either from spectroscopic line broadening or from lifetime data at lower $n(<n_M)$. Our first applications of the effective Hamiltonian for realistic model systems[38,39] established the nature of doorway and escape states, the nature of time-resolved observables (i.e., the dynamics of wave packet of eigenstates, the total excited-state population probabilities, and the population probability of the doorway state), and the consequences of different (broad band and narrow band) laser excitation modes. We are currently exploring the applications of our multichannel effective Hamiltonian formalism with several doorway and escape states for the quantitative description of the dynamics of ultrahigh atomic and molecular Rydbergs in weak external electric fields, exploring the consequences of l mixing in real systems. We have provided[40] a semiquantitative description of the autoionization dynamics of high $^2P_{1/2}np'[3/2]_1$ ($n=100-280$) Rydbergs of Ar in weak ($F\simeq 0.1$ V/cm) homogeneous electric fields which undergo a ''transition'' from the onset of effective coupling to the strong mixing domain with increasing n. We are continuing this program for the exploration of Rydberg dynamics of molecules.

In this paper we present a theoretical study of the predissociation dynamics of the $nf(N^+=2)$ ($n=40-95$) and the $np(N^+=0)$ ($n=70-125$) Rydberg series of NO, which were experimentally studied by Vrakking and Lee[10] by the time-resolved ion counting PFI method, following one-photon excitation from the intermediate $A\ ^2\Sigma^+$ ($N_A=0$, $J_a=1/2$) state. Simplified calculations of Stark mixing in the Rydbergs of NO were provided by Vrakking and Lee in the context of the analysis of their experimental data.[10] The important experimental study of Vrakking and Lee[10] interrogated the dynamics of high Rydbergs below the first ($N^+=0$) ionization potential. The novel features of the time-resolved ion counting PFI method of Vrakking and Lee[10] are

(i) High spectral resolution ($\Delta\omega_p\simeq 5\times 10^{-3}$ cm^{-1}) in conjunction with high temporal resolution (>1 ns). This technique is superior to the broad band ($\Delta\omega_p=0.1-1$ cm^{-1}) excitation mode utilized in previous studies of high Rydberg dynamics.[8,9,12–14]

(ii) The interrogation of the dynamics of the lower $n(<n_M)$ and the higher $n(>n_M)$ Rydbergs was conducted by the same experimental method. This approach is superior to previous studies of the internal conversion or/and autoionization dynamics of large molecules[9] and of autoionization dynamics in atoms,[12,13] where different methods were applied for the exploration of lifetimes in different n domains, i.e., line broadening for lower $n(<n_M)$ and time-resolved ZEKE spectroscopy for high $n(>n_M)$.

The dramatic experimental lifetime lengthening of the bound $np(N^+=0)$, $np(N^+=1)$, $nf(N^+=2)$, $nf(N^+=1)$ series of NO,[10] which correspond to predissociation dynamics in a bound electronic level structure (i.e., below the lowest $N^+=0$ ionization potential), were obtained under collision (with ions or Rydbergs)-free conditions and attributed[10] to the effects of l mixing.[38–40,44–47] The experimental data[10] for the predissociation dynamics of the $nf(N^+=2)$ and $np(N^+=0)$ high Rydbergs of NO will be confronted with the results of the theoretical study based on the multichannel effective Hamiltonian formalism.[39,40]

Our theoretical treatment requires input information on the quantum defects and decay widths parameters. Since the experimental discovery by Miescher in 1966[48] of quantum defects in the Rydberg series of a molecule, the NO molecule served as a popular hunting ground for the experimental[3,4,10,37,48–64] and theoretical[10,37,45,59,65–67] studies of Rydberg spectroscopy, predissociation and autoionization dynamics. Our analysis will provide the following results:

(i) The elucidation of the gross features of the spectra and the lifetime data for the $nf(N^+=2)$ and the $np(N^+=0)$ Rydberg series of NO in terms of the multichannel effective Hamiltonian for l mixing in a weak ($F=0.04-0.08$ V/cm) electric field.

(ii) A proper interpretation of the abnormal lifetime lengthening of the $92p(N^+=0)$ and the $95p(N^+=0)$ Rydbergs, which correspond to $n<n_M=116$ for this series.[10] This effect is attributed to perturbations originating from near-resonant sequential Rydberg electron–core dipole coupling and electric field coupling, which are subjected to strict selection rules. These resonances are treated by the effective Hamiltonian formalism, which contains both intramolecular and exterior electric field effects.

II. ENERGETICS AND DYNAMICS OF NO RYDBERGS

A. Level structure and decay widths

We shall first specify the field-free level structure and the decay widths for high n Rydberg manifold(s) of the NO molecule. As n increases the electronic angular momentum $\mathbf{l}$ is weakly coupled to the rotational angular momentum $\mathbf{N}^+$ of the NO^+ molecular core, whereupon the system is characterized by Hund's coupling case (d). The total angular momentum (excluding the spin) is $\mathbf{N}=\mathbf{l}+\mathbf{N}^+$ with a projection M_N. As the NO^+ core corresponds to a closed shell $^1\Sigma^+$ state we can limit ourselves to the treatment of $\mathbf{N}$ rather than the total angular momentum $\mathbf{J}=\mathbf{N}+\mathbf{S}$, which includes the spin angular momentum $\mathbf{S}$. The Rydberg electron–core rotational states of a definite N are[37,68,69]

$$|\kappa\rangle=|n,l,N^+,N,M_N\rangle \tag{2.1}$$

with the energies $E(\kappa)$ being given by

$$E(\kappa)=\mathrm{IP}(N^+)-\frac{\mathrm{Ry}}{(n-\delta(l,N^+))^2}, \tag{2.2}$$

where $\delta(l,N^+)$ is the quantum defect, which depends on l and also weakly on N^+.[10,37] Within the framework of Hund's coupling case (b), the quantum defect also depends on the projection of the Rydberg electron angular momentum in the molecular axis (i.e., $\sigma,\pi,\delta\cdots$states)[51,54,60] and these results will be subsequently used (Sec. 3 B) for some estimates of $\delta(l)$ for the coupling case (d). IP(N^+) is the ionization potential corresponding to the N^+ state of NO^+, which is

$$\mathrm{IP}(N^+)=\mathrm{IP}(0)+BN^+(N^++1), \tag{2.3}$$

where $B=1.9842\ \mathrm{cm}^{-1}$ is the rotational constant of the NO^+ core[10] and $\mathrm{IP}(0)=30\,522.443\ \mathrm{cm}^{-1}$ (above $A\ ^2\Sigma^+(N_A=0, J_A=1/2)$) is the lowest ionization potential converging to $N^+=0$. We shall examine the nl ($l=0-3$ and $l>3$) $N^+=0-3$ Rydberg series of NO, which correspond to electronically bound states below IP(0). The zero-order manifold $\{|\kappa\rangle\}$ is subdivided into three submanifolds:

(i) Doorway states. A subset of low l ($l=0-3$) core-penetrating states constitutes the doorway states for excitation. These doorway states are determined by the optical excitation conditions and selection rules, e.g., one-photon excitation, two-photon excitation, or excitation from an intermediate state. We shall be interested in one-photon excitation from the $A\ ^2\Sigma^+(N_a=0,J_a=1/2)$ intermediate state of NO, resulting in the $nf(N^+=2)$ and $np(N^+=0)$ doorway states.[10]

(ii) Escape states. The doorway state and additional low $l(\leqslant 3)$ states, which are coupled to it by Stark coupling (and in some rare cases, which are discussed in Sec. IV, also by near-resonant intramolecular Rydberg electron-core coupling) constitute the escape states for the decay. For the states of NO below IP(0) the escape states are coupled to the predissociation decay channels and are characterized by decay widths, Eq. (1.2). These decay widths of the $|\kappa\rangle$ states $\{\Gamma_\kappa(n)\}$ are characterized by the decay width constants $\Gamma_0(l,\alpha)$ ($\alpha=N^+$), with Γ_0 essentially depending on l, and being given by the scaling law, Eq. (1.2) $\Gamma_\kappa(n)=\Gamma_0(l,N^+)/[n-\delta(l,N^+)]^3$.

(iii) The inactive manifold. The high $l(\geqslant 4)$ nonpenetrating hydrogenic states (which will be denoted by $|L\rangle$), are inactive in excitation and in decay. For these states $\delta(L)=0$ and $\Gamma_0(L)=0$.

B. Interactions

The level structure in the unperturbed Hund coupling case (d) consists of ''l complexes'' at each value of the core rotation quantum number N^+ with $(2l+1)$ degenerate sublevels with different values of N (for $N^+\geqslant l$). Figure 1 shows the $l(=0-3)$ complexes for $N^+=0-3$. The coupling between $|n,l,N^+,N\rangle$ and $|n'l',N^{+'},N\rangle$ states involves two types of interactions, both of which are subjected to strict selection rules:

(i) Intramolecular Rydberg electron–core dipole long-range interactions.[69–73] These will be shown to be small relative to the level spacing in most cases, except for some accidental near-resonances. Furthermore, we shall demonstrate that these intramolecular interactions may prevail only within the submanifolds of the core-penetrating low $l(\leqslant 3)$ Rydbergs, i.e., between some of the doorway and escape states and do not couple the low $l(\leqslant 3)$ manifolds with the inactive $(l\geqslant 4)$ states. Accordingly, intramolecular coupling is ineffective for l mixing.

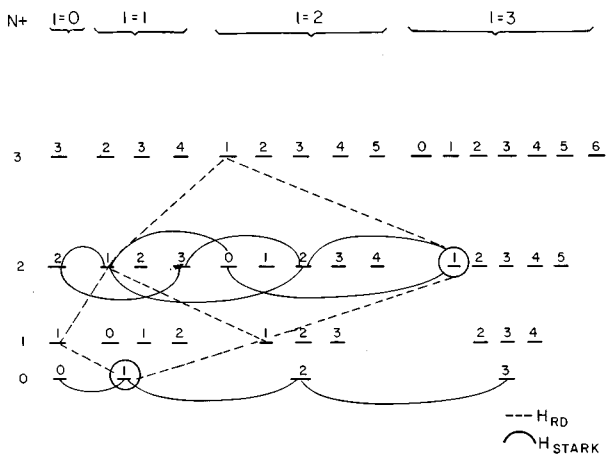

FIG. 1. A schematic diagram of the s,p,d, and f complexes ($l=0-3$) for the first few core rotation levels (core rotation quantum numbers $N^+=0-3$) in the Hund coupling case (d). Each column of $(2l+1)$ levels marked by l represents a single l complex, while the states in each line marked by N^+ represent different rotational levels. The numbers on the horizontal lines label the total angular momentum N (excluding the spin). The two doorway states $np(N^+=0)$ and $nf(N^+=2)$ are marked by a circle. Dashed lines represent the intramolecular Rydberg electron-core dipole coupling ($H_{\mathrm{R\text{-}D}}$) subjected to the selection rules (2.10), while solid lines represent the electric field coupling H_{STARK} subjected to the selection rules (2.16).

(ii) Electric field couplings induced by a weak homogeneous electric field $F(\simeq 0.01–0.3\ \mathrm{V/cm})$. These exterior couplings dominate the dynamics via l mixing.

Neglecting the decay channels, the Hamiltonian of the diatomic molecule in the presence of a homogeneous electric field is

$$\mathscr{H}_M=\mathscr{H}_0+\mathscr{H}_{\mathrm{R\text{-}D}}+\mathscr{H}_{\mathrm{STARK}}, \tag{2.4}$$

where the zero-order molecular Hamiltonian for Hund's case (d) is

$$\mathscr{H}_0=\sum_\kappa |\kappa\rangle E_\kappa\langle\kappa| \tag{2.5}$$

being expressed in terms of Eqs. (2.1)–(2.3). $H_{\mathrm{R\text{-}D}}$ is the Rydberg electron–molecular dipole coupling[69–73]

$$\mathscr{H}_{\mathrm{R\text{-}D}}=\frac{e}{r^2}\,\mathbf{C}^{(1)}(\theta,\phi)\cdot\boldsymbol{\mu}, \tag{2.6}$$

where r,θ,ϕ are the Rydberg electron coordinates in the molecule-fixed coordinate system, $\mathbf{C}^{(1)}(\theta,\phi)$ is the angular vector,[74] and $\boldsymbol{\mu}$ is the (electronic origin independent) dipole moment of the NO^+ ion. In this analysis only the $H_{\mathrm{R\text{-}D}}$ term was incorporated in the intramolecular long-range interaction, which also includes the Rydberg electron–core quadrupole and (anisotropic) polarizability couplings.[69,70] A detailed (yet unpublished) analysis of the intramolecular dipole, quadrupole, and polarizability couplings for NO indicates that it is dominated by $H_{\mathrm{R\text{-}D}}$. We also note in passing

that the quantum defects incorporate two contributions: (a) The effects of core penetration.[76] (b) The diagonal matrix elements of the long-range quadrupole and polarizability interactions.[69,70,75]

Finally, $\mathscr{H}_{\mathrm{STARK}}$ is the Stark Hamiltonian

$$\mathscr{H}_{\mathrm{STARK}} = -e\mathbf{r}\cdot\mathbf{F}. \tag{2.7}$$

We have now to consider the selection rules and the matrix elements between the $\{|\kappa\rangle\}$ states for the intramolecular coupling, Eq. (2.6), and the field induced coupling, Eq. (2.7).

C. Intramolecular coupling and the bottleneck effect

The matrix elements for the Rydberg electron–core dipole coupling are[69–72]

$$\langle n,l,N^+,N,M_N|H_{\mathrm{R\text{-}D}}|n',l',N^{+'},N',M_N'\rangle = -e\mu\langle \nu l|r^{-2}|\nu' l'\rangle \otimes f(l,N^+,N,M_N;l',N^{+'},N',M_N'), \tag{2.8}$$

where $\nu = n-\delta(l)$ while the angular part is

$$f(l,N^+,N,M_N;l',N^{+'},N',M_N') = (-1)^{l'+l+N'}\begin{Bmatrix} N' & N^+ & l \\ 1 & l' & N^{+'} \end{Bmatrix} \otimes \delta_{N,N'}\delta_{M_N,M_N'}[(2l+1)(2l'+1)]^{1/2}\begin{bmatrix} l & 1 & l' \\ 0 & 0 & 0 \end{bmatrix} \otimes [(2N^+ +1)(2N^{+'}+1)]^{1/2}\begin{bmatrix} N^+ & 1 & N^{+'} \\ 0 & 0 & 0 \end{bmatrix} \tag{2.9}$$

with the selection rules

$$\Delta l = \pm 1, \quad \Delta N^+ = \pm 1, \quad \Delta N = 0, \quad \Delta M_N = 0, \tag{2.10}$$

while there is, of course, no constraint on $\Delta\nu$ (or Δn). The ΔN, ΔN^+, and Δl selection rules, Eq. (2.10), imply that the intramolecular coupling occurs between members of l complexes which differ by a unit of N^+, with N being conserved. In Fig. 1 we present examples for the schemes of intramolecular coupling from the $nf(l=3,N^+=2,N=1)$ and from the $np(l=1,N^+=0,N=1)$ doorway states experimentally studied by Vrakking and Lee.[10]

We first explore the energetics and coupling of the proximal (closest lying) pairs of energy levels of low l (i.e., core penetrating) doorway and escape Rydberg states, which are subjected to the selection rules, Eq. (2.10). These energy gaps between proximal pairs of energy levels will be subsequently compared with semiquantitative estimates for the strength of the intramolecular coupling, Eq. (2.8), between these pairs of high Rydbergs. Regarding the energetics, we have examined the energy gaps $|E(n,l,N^+,N) - E(n',l',N^{+'},N')|$ for $n=40-120$ (where n' is chosen to provide the smallest energy gap for this pair of states) with $l',N^{+'},N'$ subjected to the selection rules (2.10), exploring the core penetrating states $l=0-3$ and $N^+=0-3$. Typical data for the energy gaps

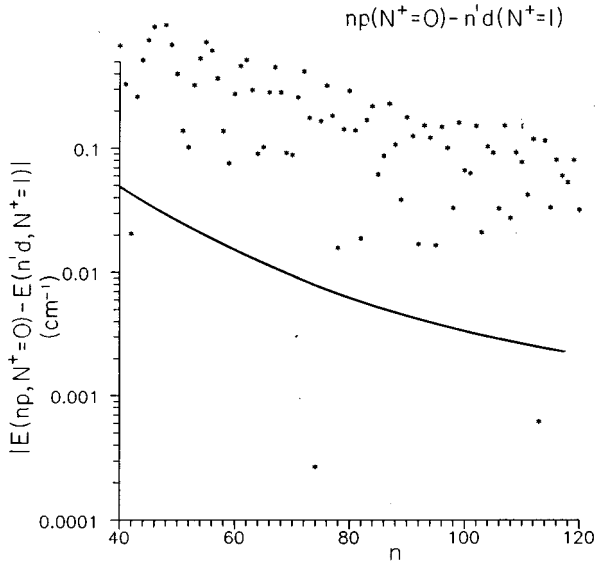

FIG. 2. Energetics and coupling of proximal $np(N^+=0)$ and $n'd(N^+=1)$ energy levels. The energy gaps between the $np(N^+=0)$ state ($N=40-120$) and the closest lying $n'p(N^+=1)$ state are marked by a point for each value of n. The solid line represents the intramolecular coupling matrix element, Eq. (2.9), with the radial integral being represented by the near threshold approximation with phase shifted wave function, Eq. (2.11), $|\langle n,l=1,N^+=0|H_{\mathrm{R\text{-}D}}|n'l=2,N^+=1\rangle| = 3.2\times10^3(nn')^{-3/2}$ cm^{-1}.

$|E(n,l=1,N^+=0)-E(n',l'=2,N^{+'}=1)|$ for the proximal $np(N^+=0)$ and $n'd(N^+=1)$ pairs of states are presented in Fig. 2. From these results we conclude that the majority of the energy gaps are large, i.e., $\Delta E > 2\times10^{-2}$ cm^{-1}. There are only a few accidental near-resonances between proximal pairs of states, e.g., out of 80 energy gaps in Fig. 2 we identified two extremely small energy gaps ($>10^{-3}$ cm^{-1}) and five moderate energy gaps ($\sim 2\times10^{-2}$ cm^{-1}), while all the other gaps are substantially larger.

The energy gaps have to be compared with the strengths of the intramolecular coupling for high Rydbergs. A semiquantitative estimate of the $\langle n,l,N^+,N|H_{\mathrm{R\text{-}D}}|n',l',N^{+'},N'\rangle$ coupling, Eq. (2.10), for high n,n' states was obtained utilizing the Gilbert–Child[72] near-threshold approximation with a finite quantum defect for the radial integral in Eq. (2.10)

$$\langle \nu l|r^{-2}|\nu' l'\rangle = 2(\nu\nu')^{-3/2}(\lambda+\lambda'+1)^{-1}\frac{\sin[\pi(\lambda-\lambda')]}{\pi(\lambda-\lambda')}, \tag{2.11}$$

where $\lambda = l-\delta(l)$ is the effective azimuthal quantum number and again $\nu = n-\delta(l)$. Equation (2.11) is based on the asymptotic form of the phase shifted radial wave function.[72] A major contribution to the radial integral, Eq. (2.11), for high n and n' states originates from very short distances (i.e., $r \leqslant 4$ a.u. for the $np-n'd$ interaction, $n,n'=80-100$), in accord with Berry's classical studies of molecular autoionization.[31] Accordingly, the utilization of Eq. (2.11) constitutes only an approximate description, which is, however, sufficient for our purposes. Making use of Eqs. (2.8) and (2.11) the (absolute value) of the

matrix element $|\langle H_{\text{R-D}}\rangle|$ between the $np(N^+=0)$ and $n'd(N^+=1)$ proximal pairs of energy levels is $|\langle H_{\text{R-D}}\rangle| \simeq 3.2\times 10^3 n^{-3/2}(n')^{-3/2}$ cm^{-1}, which is presented in Fig. 2. From Fig. 2 we conclude that in the majority of cases $|\langle H_{\text{R-D}}\rangle| \ll |E(np,N^+=0)-E(n'd,N^+=1)|$ and only a few accidental near-resonant couplings are exhibited between proximal pairs of states. Similar results were obtained for the energetics and couplings of other pairs of Rydbergs. From this analysis we conclude that intramolecular near-resonant couplings between core-penetrating high Rydberg states are scarce. The few accidental near-resonance couplings between low l Rydbergs have two manifestations.

(i) Intramolecular mixing of pairs of states. In the hypothetical case of the absence of any (stray or imposed) electric field ($F=0$) mixing of pairs of states characterized by extremely small energy gaps $|E(nlN^+)-E(n'l'N^{+\prime})| \leqslant |\langle H_{\text{R-D}}\rangle|$ will be exhibited, resulting in the redistribution of the decay widths between the pair of states. Such local perturbations may result in either shortening or lengthening of the lifetimes of a doorway state, depending on the decay widths of the corresponding $|nlN^+\rangle$ and the $|n'l'N^{+\prime}\rangle$ states.

(ii) Mediation by intramolecular coupling. In the presence of a weak electric field some $|n'l'N^{+\prime}\rangle$ states characterized by modest energy gaps, i.e., $|E(nlN^+) - E(n'l'N^{+\prime})| \simeq |\langle H_{\text{R-D}}\rangle|$ act as mediating states for the electric field induced coupling of the doorway state $|nlN^+\rangle$ to the inactive $|n'l''(>3)N^{+\prime}\rangle$ manifold. An additional necessary condition for such mediated coupling is near degeneracy between the doorway $|nlN^+\rangle$ state and the $|n'l''(>3)N^{+\prime}\rangle$ manifold. Two notable such mediated couplings involve the $92p$-$80d$-$80l''(>3)$ and the $95p$-$82d$-$82l''(>3)$ manifolds,[10] which will be discussed in Sec. IV.

We proceed to the coupling with and within the inactive $|L\rangle$ manifold of high $l(>3)$ states, which is subjected to the selection rules (2.10). Nonpenetrating Rydberg states with $\delta(l)=0$ are hydrogenic. A general relation of Laguerre polynomials[77] implies that for radial hydrogenic wave functions within a single n manifold $\langle n,l|r^{-(p+1)}|n,l\pm p\rangle = 0$ for integer $p \geqslant 1$. Accordingly, for the inactive $|L\rangle$ manifold

$$\langle n,l|r^{-2}|n,l\pm 1\rangle = 0; \quad \delta(l)=0. \tag{2.12}$$

The exact result, Eq. (2.12), is consistent with the results of an approximate analysis based on the near-threshold approximation, Eq. (2.11). In the high $l(>3)$ regime $\delta(l)\to 0$ with increasing l and $(\lambda-\lambda')\to(l-l')+O(\delta(l)-\delta(l')) = \pm 1 + O(\delta(l)-\delta(l\pm 1))$. In this domain we expect that $\delta(l)$ decreases fast with increasing l, i.e., $\delta(l)\propto l^{-5}$,[78–80] whereupon $\delta(l)-\delta(l')\propto 5l^{-6}$. We infer that the radial integral for large n and l values, Eq. (2.11) decreases fast towards zero with increasing l, being of the form $l^{-1}\sin[5\pi A/l^6]$, where A is a numerical constant, i.e.,

$$\langle \nu,l|r^{-2}|\nu',l\pm 1\rangle \propto l^{-7}; \quad l>3. \tag{2.13}$$

Accordingly, the near threshold limiting (high n) condition for the inactive $\{|L\rangle\}$ manifold ($\delta(l)=0$) is

$$\langle nl|r^{-2}|n'l\pm 1\rangle = 0; \quad \delta(l)=0. \tag{2.12a}$$

Equation (2.12a) for the asymptotic near threshold form is consistent with the exact relation, Eq. (2.12). We note in passing that while the exact expression [Eq. (2.12)] implies the vanishing of the integrals only within the same n manifold, the asymptotic expression, Eq. (2.12a), also implies the vanishing of the integrals between different n manifolds, as the r dependence of the near-threshold wave functions is determined only by l.

From Eqs. (2.12) and (2.13) [which obey the appropriate selection rules (2.10)] it is apparent that the intramolecular Rydberg electron–core dipole couplings decrease fast ($\propto l^{-6}$) towards zero with increasing $l(>3)$. Concurrently we found (from a simple numerical analysis) that the energy gaps between proximal $nl-n'(l+1)$ pairs of energy levels ($l>3$), which are characterized by different n values and obey the selection rules (2.10), remain large (mostly $>10^{-2}$ cm^{-1}) and irregular. We thus conclude that intramolecular Rydberg electron–core dipole coupling cannot involve the $nl-n'(l+1)$ mixing of higher l states (with $n\neq n'$) within the inactive $\{|L\rangle\}$ manifold. Accordingly, the fast decrease of the radial integrals for intramolecular coupling exhibits a bottleneck effect, which precludes the intramolecular mixing of higher $l(>3)$ states (with $n\neq n'$) within the inactive $\{|L\rangle\}$ manifold. It is important to emphasize that this demonstration of the bottleneck effect depends only on the characteristics of the nonpenetrating high $l(>3)$ states, which are invariant with respect to the magnitude of the rotational constant, being expected to occur both in a diatomic molecule, e.g., NO, and for a large molecule.

Returning to the level structure and couplings of the field-free NO Rydbergs (Figs. 1 and 2 and Table I) we conclude that:

(i) In the low $l(<4)$ domain of doorway and escape states of NO only a small number of accidental near-resonances is exhibited.

(ii) In the high inactive $\{|L\rangle\}$ manifold ($l\geqslant 4$) the bottleneck effect precludes intramolecular l mixing (between different n states, according to the selection rule $\Delta N^+ = \pm 1$ for dipole coupling). Accordingly, in the field-free NO molecule (and also for any other diatomic or a large molecule) the $\{|L\rangle\}$ states retain their identity.

From this analysis we conclude that, apart from a small number of low l near-resonances which have to be treated separately (see Sec. IV), the dynamics of the high Rydberg states of NO is practically unaffected by the intramolecular Rydberg electron–core dipole coupling and is dominated by the Stark coupling, which will now be considered.

D. Stark coupling

The matrix elements for the Stark coupling, Eq. (2.7), are of the same form as those for the electric dipole matrix elements, being (for the $M_N=0$ component)[69,74]

$$\langle \nu,l,N^+,N,M_N|H_{\text{STARK}}|\nu',l',N^{+\prime},N',M_N'\rangle = e\langle \nu,l|r|\nu',l'\rangle G(l,N^+,N,M_N;l',N^{+\prime},N',M_N')F, \tag{2.14}$$

where

$$G(l,N^+,N,M_N;l',N^{+\prime},N',M_N') = (-1)^{N-M_N}\begin{bmatrix} N & 1 & N' \\ -M_N & 0 & M_{N'} \end{bmatrix} \otimes (-1)^{N^{+\prime}+l'+N+1} \times [(2N+1)(2N'+1)]^{1/2}\begin{Bmatrix} l & N & N^{+\prime} \\ N' & l' & 1 \end{Bmatrix} \otimes (-1)^{l}[(2l+1)(2l'+1)]^{1/2}\begin{bmatrix} l & 1 & l' \\ 0 & 0 & 0 \end{bmatrix} \quad (2.15)$$

with the selection rules

$$\Delta l = \pm 1, \quad \Delta N^+ = 0, \quad \Delta N = \pm 1, 0 (0 \leftrightarrow 0), \quad \Delta M_N = 0, \pm 1. \quad (2.16)$$

These ΔN, ΔN^+, and Δl selection rules imply that the Stark coupling occurs between members of l complexes with the same value of N^+, while N can be changed by unity. Figure 1 presents examples for the scheme of Stark coupling from the $nf(l=3,N^+=2,N=1)$ and from the $np(l=1,N^+=0,N=1)$ doorway states.

The radial matrix elements in Eq. (2.14) are evaluated for different l dependent quantum defects [which result in the l dependent effective quantum number $\nu = n - \delta(l)$], using the formula of Edmonds *et al.*[81]

$$\langle \nu l | r | \nu' l' \rangle = (3\nu_c^2 a_0/2)\left(1 - \left(\frac{l_c}{\nu_c}\right)^2\right)^{1/2} \sum_{\mu=0}^{3} \gamma^{\mu} g_{\mu}(\Delta\nu), \quad (2.17)$$

where

$$l_c = \max(l,l'), \quad \nu_c = \frac{2\nu\nu'}{(\nu+\nu')}, \quad \Delta l = (l-l'),$$

$$\gamma = \Delta l\left(\frac{l_c}{\nu_c}\right), \quad \Delta\nu = \nu - \nu'. \quad (2.17a)$$

The functions $g_{\mu}(\Delta\nu)$ were tabulated by Edmonds *et al.*[81]

E. Isolated and overlapping *n* rydberg manifolds

A single Rydberg manifold (which will be referred to as a single n manifold), will be chosen to contain a set of zero-order states with the closest ν values. Such a single n manifold will be characterized as follows:

(i) The nl hydrogenic states for the $\{|L\rangle\}$ submanifold.

(ii) The $\nu l(\nu = n - [(2\delta(l))(\mathrm{mod}1) - \delta(l)(\mathrm{mod}1)]$ doorway and escape states for which $\delta(l) \neq 0$. These latter states correspond to the principal quantum number $\nu = n + \delta(l) - \delta(l)(\mathrm{mod}1)$.

Overlap between neighboring n manifolds is realized when the energetic spread $\Delta W(\mathrm{cm}^{-1}) = 6\ \mathrm{Ry} n^2 F/(5.15\times 10^9) = 1.3\times 10^{-4} n^2 (F/\mathrm{V\ cm}^{-1})$ of a single hydrogenic Stark manifold exceeds the intermanifold spacing $2\ \mathrm{Ry}/n^3$, i.e., $\Delta W/2 > 2\ \mathrm{Ry}/n^3$. Intermanifold overlap then occurs for $n > 80.6(F/\mathrm{V\ cm}^{-1})^{-1/5}$, which constitutes the Inglis–Teller relation with slightly modified numerical constants. A more pedantic argument for the Stark splitting of a manifold consisting of a doorway (and escape) state with a quantum defect $\delta(l)$ and an inactive $\{|L\rangle\}$ manifold implies that $\Delta W/2 > 2R/n^3 - 2R\delta/n^3$. Intermanifold overlap then occurs for

$$n > 80(1-\delta)^{1/5}(F/\mathrm{V\ cm}^{-1})^{-1/5}, \quad (2.18)$$

introducing the dependence on the quantum defect in the Inglis–Teller relation. For the $nf(N^+=2)$ series, the quantum defect is small $[\delta(f)=0.0101]$ so that $n>145$ for $F=0.05$ V/cm and calculations for $n=40-95$ [below the first ionization potential IP(0)] were performed for a single isolated n manifold. For the $np(N^+=0)$ series where $\delta(p)=0.729$ we determine $n \geqslant 110$. In view of the approximate nature of this estimate we have conducted the calculations for the np series with $n \geqslant 100$ employing three neighboring n manifolds and picking up the level structure from the middle portion of the spectrum.

F. The effective Hamiltonian

Up to this point we have been concerned with the energy spectrum of the Hamiltonian $\mathscr{H}_M$, Eq. (2.4), below the first ionization potential IP(0) and disregarding the effects of predissociation. The NO Rydberg level structure and predissociation dynamics are determined by the effective Hamiltonian[22–25,38–40]

$$\mathscr{H}_{\mathrm{eff}} = \mathscr{H}_0 + \mathscr{H}_{\mathrm{R\text{-}D}} + \mathscr{H}_{\mathrm{STARK}} - (i/2)\mathbf{\Gamma}, \quad (2.19)$$

where $\mathbf{\Gamma}$ is the decay matrix of the doorway state(s) and of the other escape states. In the absence of intermanifold overlap when a single n manifold is sufficient, a single (np or nf) doorway state denoted by $|D\rangle$ and several (β) pure escape states denoted by $|E\beta\rangle$ ($\beta = 1 \text{---} \beta$) are characterized by finite decay widths $\Gamma_{l,N^+}(n)$. In the case of overlap of neighboring n manifolds there are several ($\overline{\alpha}$) doorway states [i.e., $(n-1)p$, np and $(n+1)p$], denoted by $|D\alpha\rangle$ ($\alpha = 1 \text{---} \overline{\alpha}$) and several ($\beta$) pure escape states $|E\beta\rangle$ ($\beta = 1 \text{---} \beta$). The diagonal matrix elements of $\mathbf{\Gamma}$, which are given by $\Gamma_{l,N^+}(n)$ are inferred from the decay width constants $\Gamma_0(l,N^+)$ (Table I) using the n^3 scaling law, Eq. (1.2).

Following the analysis of the intramolecular coupling (Sec. II C) we infer that for most cases near-resonant level interactions via $H_{\mathrm{R\text{-}D}}$ subjected to strict selection rules, Eq. (2.10), are absent. The effective Hamiltonian for the NO Rydbergs and can be reduced to

$$\mathscr{H}_{\mathrm{eff}} = \mathscr{H}_0 + \mathscr{H}_{\mathrm{STARK}} - (i/2)\mathbf{\Gamma}. \quad (2.20)$$

This effective Hamiltonian will be utilized in Sec. III for the treatment of field-induced l mixing in the case of excitation of $np(N^+=0)$ or $nf(N^+=2)$ doorway states. For the case of near-resonant interactions the full-fledged effective Hamiltonian, Eq. (2.19), will be utilized in Sec. IV.

The effective Hamiltonian, Eq. (2.19) or (2.20), can be diagonalized by a complex orthogonal transformation, resulting in the independently decaying levels $|j\rangle$ of the system. For the situation of intermanifold overlap, when several doorway states (corresponding to different neighboring n values) are mixed, the $\{|j\rangle\}$ levels are

$$|j\rangle=\sum_{\alpha=1}^{\overline{\alpha}} a_{\alpha}^{(j)}|D\alpha\rangle+\sum_{\beta=1}^{\overline{\beta}} a_{\beta}^{(j)}|E\beta\rangle+\sum_{n}\sum_{l>3} b_{n,l}^{(j)}|nl\rangle, \tag{2.21}$$

where $\{a_{\alpha}^{(j)}\}$, $\{a_{\beta}^{(j)}\}$ and $\{b_{n,l}^{(j)}\}$ are (complex) coefficients. For a single n manifold, when a single doorway state $|D\alpha\rangle$ contributes we have

$$|j\rangle=a_{\alpha}^{(j)}|D\alpha\rangle+\sum_{\beta=1}^{\overline{\beta}} a_{\beta}^{(j)}|E\beta\rangle+\sum_{l>3} b_{l}^{(j)}|l\rangle. \tag{2.22}$$

The (complex) eigenvalues of the system are

$$\in_j=E_j-(i/2)\gamma_j, \tag{2.23}$$

where E_j are the energy levels and γ_j the decay widths (reciprocal lifetimes) of the $|j\rangle$ eigenstates. The experimental input parameters required for the construction of the effective Hamiltonian at a constant field F are:

(i) the quantum defects $\delta(D\alpha)$ and $\delta(E\beta)$, extracted from the Rydberg series energetics, and

(ii) the decay width constants $\Gamma_0(D\alpha)$ and $\Gamma_0(E\beta)$, obtained from the linewidths or decay times of the lower Rydberg levels.

G. Excited-state total population probability for different excitation modes

We shall be concerned with the excitation and decay (the rise and fall) of the mixed level structure of a single n manifold, Eq. (2.22), or several n manifolds, Eq. (2.21), which are subjected to l mixing. To make contact with experiment, we consider the dynamics of the excited state total population probability $P(t)$,[38] which corresponds either to the time dependent population of a subset of $\{|j\rangle\}$ states prepared by narrow-bandwidth laser excitation[38] or the total set of $\{\{|j\rangle\}\}$ states prepared by broad band laser excitation.[38–40] In particular, we shall be interested in the treatment of the dynamics under narrow band excitation conditions, for which the theoretical framework was already given,[38] and which was experimentally explored for NO Rydbergs by Vrakking and Lee.[10] Some results for the Rydberg dynamics under broad band (low-resolution) excitation conditions will be presented for the sake of comparison.

Consider the excitation (predissociative) decay of a single n manifold. We follow our analysis[38] for a sparse level structure, i.e., $\gamma_j/|E_j-E_{j'}|\ll 1$ for all j and j', a condition well satisfied for the np and nf Rydberg series of NO (Table I).

The conditions for narrow band excitation are realized when the laser bandwidth $\Delta\omega_p$ is considerably narrower than the total Stark width ΔW, while the linewidths (reciprocal lifetimes) γ_j of the individual mixed states are considerably narrower than $\Delta\omega_p$, i.e.,

$$\Delta\omega_p\ll\Delta W;\quad \Delta\omega_p\gg\gamma_j. \tag{2.24}$$

Under these excitation conditions a wavepacket of several eigenstates $\{j\}$ is excited. The total population probability consists of several exponential decay terms[38]

$$P(t)=\sum_{\{j\}}|a_{\alpha}^{(j)}|^2F_j(\overline{E},\Delta\omega_p)\exp(-\gamma_j t), \tag{2.25}$$

where $F_j(\overline{E},\Delta\omega_p)$ is the weight of the line shape of the laser pulse with a central energy $\overline{E}$, which is given either by a Lorentzian form

$$F_j(\overline{E},\Delta\omega_p)=\frac{(\Delta\omega_p)^2}{(\overline{E}-E_j)^2+\Delta\omega_p^2} \tag{2.26}$$

or by a Gaussian form

$$F_j(\overline{E},\Delta\omega_p)=\frac{1}{(2\pi\Delta\omega_p^2)^{1/2}}\exp[-(\overline{E}-E_j)^2/(2\Delta\omega_p)^2]. \tag{2.27}$$

Next we consider the broad band excitation conditions

$$\Delta\omega_p\gg\Delta W. \tag{2.28}$$

Taking $\Delta W=1.3\times10^{-4}n^2(F/\mathrm{V\ cm^{-1}})$ and $\Delta\omega_p=0.1$–1.0 $\mathrm{cm^{-1}}$ for typical multimode lasers, condition (2.28) is obeyed, e.g., for $F=0.05$ V/cm $n\leqslant220$ (for $\Delta\omega_p=0.3$ $\mathrm{cm^{-1}}$) and $n\leqslant130$ (for $\Delta\omega_p=0.1$ $\mathrm{cm^{-1}}$). The broad band excitation (of the sparse manifold of the mixed j levels) results in the time dependent population probability

$$P^{\mathrm{BB}}(t)=\sum_j|a_{\alpha}^{j}|^2\exp(-\gamma_j t). \tag{2.29}$$

Equations (2.25) and (2.26) correspond to a single doorway state when the dynamics of a single n manifold can be considered. For the case of the decay of several overlapping n manifolds, these equations have to be modified. For the narrow band excitation

$$P(t)=\sum_{\{j\}}\sum_{\alpha=1}^{\overline{\alpha}}|d_{\alpha}a_{\alpha}^{(j)}/(E_j-\overline{E}-(i/2)\Delta\omega_p)|^2\exp(-\gamma_j t), \tag{2.25a}$$

while for the broad band excitation

$$P^{\mathrm{BB}}(t)=\sum_j\left|\sum_{\alpha}d_{\alpha}a_{\alpha}^{(j)}\right|^2\exp(-\gamma_j t), \tag{2.29a}$$

where d_{α} is the transition moment for the excitation of the doorway state $|D\alpha\rangle$. We note that temporal coherence effects, i.e., quantum beats, are not exhibited in the total decay probability for all the excitation modes.[38] Energetic interference effects are revealed when several doorway states are involved.

H. Experimental observables

The theoretical results for $P(t)$, Eqs. (2.25), and $P^{\mathrm{BB}}(t)$, Eq. (2.29), make contact with experimental reality. In view of the novel narrow bandwidth experimental conditions utilized by Vrakking and Lee,[10] the narrow band limit, Eq. (2.25), has to be utilized for the exploration of the time-resolved dynamics:

(i) The time-resolved total population probability under the conditions of narrow band excitation in the vicinity of the maximum of the PFI spectrum.

(ii) Lifetimes of the mixed high Rydbergs can be inferred from the time scales for the temporal decay of $P(t)$. These theoretical results for narrow band excitation can be confronted with the experimental data for lifetimes using delayed PFI.

Apart from time-resolved observables, energy-resolved PFI spectra can be calculated. The line shape $L(E)$ at the laser energy E is obtained from the spectrum of the weights $|a_\alpha^{(j)}(E)|^2$ of the doorway states averaged over the laser energetic envelope

$$L(E)=\sum_j |a_\alpha^{(j)}(E)|^2 F_j(E,\Delta\omega_p). \tag{2.30}$$

These calculated PFI spectra will be confronted with the experimental data.

III. THE DYNAMICS OF NO PREDISSOCIATION IN WEAK ELECTRIC FIELDS

A. Strategy

Our calculation of the predissociation dynamics will be based on:

(i) The construction of the multichannel effective Hamiltonian (Secs. III A–III C) for the predissociation of NO Rydbergs via the $nf(N^+=2)$ and $np(N^+=0)$ doorway states. Vrakking and Lee[10] studied the five Rydberg series $np(N^+=0,1)$ and $nf(N^+=1,2,3)$. We have chosen the $np(N^+=0)$ and $nf(N^+=2)$ series as generic examples. As accidental near-resonances are scarce (Sec. II C), we shall neglect in this section intramolecular coupling effects and construct the effective Hamiltonian in the form given by Eq. (2.20).

(ii) The diagonalization of the effective Hamiltonian. For the $nf(N^+=2)$ series $\mathscr{H}_{\rm eff}$ was diagonalized in the range $n=40-95$, where the upper limit of n is determined by the onset of autoionization at $\overline{n}=[\mathrm{Ry}/I(2)-I(0)]^{1/2}=95$. For the $np(N^+=0)$ series we diagonalized $H_{\rm eff}$ in the range $n=60-135$, with the upper limit of n being determined by experimental considerations of the spectral resolution of the Stark mixed Rydbergs by a weak stray field. For the nf ($n=40-95$) a single n manifold was sufficient while for the np ($n=60-125$) series in the range $n<100$ a single n manifold was used, while for $n>100$ three adjacent n manifolds $[(n-1)$, n and $(n+1)]$ were used (see Sec. II E). The calculations were performed for weak electric fields in the range $F=0.01-0.3$ V/cm.

(iii) From the complex eigenvalues and eigenvectors of the effective Hamiltonian we obtained the energies E_j of the $\{|j\rangle\}$ states (Sec. II F), the decay widths γ_j and lifetimes $\tau_j=\hbar/\gamma_j$ of the $\{|j\rangle\}$ states and the mixing coefficients $|a_\alpha^{(j)}|^2$ of the doorway state(s) within all the $|j\rangle$ states.

(iv) Calculation of $P(t)$, Eq. (2.25), for narrow band excitation, which was performed in the vicinity of the maximum of the lineshape of the PFI spectrum.[10] Some calculations of $P^{\rm BB}(t)$, Eq. (2.29), for broad band excitation were also performed.

TABLE II. Quantum defects δ and Γ_0 decay width constants data for the NO Rydbergs predissociation dynamics.

Rydberg series	δ	Γ_0 (cm^{-1})
ns	1.21[a]	(500)[e]
$np(N^+=0)$	0.7286[b]	1610[d]
nd	−0.05[a]	(1000)[e]
$nf(N^+=2)$	0.0101[b]	43[c]

[a]Quantum defect data from Refs. 51, 54, and 60.
[b]Reference 10.
[c]From the lifetime data of the $nf(N^+=2)$ series, $n=40-65$ of Ref. 10.
[d]From the lifetime data of the $np(N^+=0)$ series, $n=70-110$ of Ref. 10.
[e]From the analysis of the strong field lifetime data of Ref. 10 using the diagonal sum rule. Arbitrary partitioning of $\Gamma_0(s)+\Gamma_0(d)=1500$ cm^{-1} (see the text).

(v) Calculation of energy resolved lineshapes $L(E)$, Eq. (2.30).

B. Input data

The construction of $\mathscr{H}_{\rm eff}$, Eq. (2.20), for the predissociation of NO requires experimental information on the quantum defects and decay widths parameters of the doorway state and other escape states, which correspond to the $(l=0-3)$ ns, np, nd, and nf manifolds of the $N^+=0-3$ complexes (Fig. 1). For the inactive $\{|L\rangle\}$ ($l\geqslant 4$) Rydbergs $\delta(L)=0$ and $\Gamma_0(L)=0$. Since the pioneering studies of Miescher,[48] substantial information on the quantum defects has accumulated.[10,48–54,60,65,66] The work of Miescher, Lee, Gürtler, and Huber[51,54] on the s,p,d complexes gave $\delta(s)=1,2$, $\delta(p_\sigma)=0.68$, $\delta(p_\pi)=0.74$, $\delta(d_\sigma)\simeq\delta(d_\pi)=-0.02$ and $\delta(d_\delta)=0.07$. Subsequent work of Gauyacq *et al.*[60] on the s and d complexes gave $\delta(s_\sigma)=0.210$, $\delta(d_\sigma)=-0.049$, $\delta(d_\pi)=-0.052$ and $\delta(d_\delta)=0.089$. These quantum defects correspond to the Hund coupling case (b). Theoretical quantum defect data were given by Jungen and Raoult[65,66] for the $np\sigma$ series and confronted with the experimental data. The high resolution studies of Vrakking and Lee[10] on the np and nf series established a weak N^+ dependence of the quantum defects for the np states and a stronger N^+ dependence of the small quantum defects for $\delta(p,N^+=0)=0.7286$ and $\delta(p,N^+=1)=0.7038$, while $\delta(f,N^+=1)=0.0168$ and $\delta(f,N^+=2)=0.0101$. In Table II we present a set of l dependent quantum defect data for NO, where the $\delta(p)$ and $\delta(f)$ data rest on the high-resolution data of Vrakking and Lee,[10] while the data for s and d complexes are taken from the work of Miescher *et al.*[51,54] and of Gauyacq *et al.*[60] In these estimates of the quantum defects we represent the nl states as pure l orbitals and some effects of intramolecular l mixing (for low l values), e.g., $s-d$ mixing,[57,65(a)] which are induced by quadrupole and/or anisotropic polarizability coupling were not considered.

The spectroscopic input information on the dynamics is scarce. The predissociation channels are[61] $\mathrm{N}(^4S)+\mathrm{O}(^3P)$ at $E_{d1}=52\,400\pm400$ cm^{-1}, $\mathrm{N}(^4S)+\mathrm{O}(^1D)$ at $E_{d2}\simeq 68\,300\pm400$ cm^{-1}, and $\mathrm{N}(^2D)+\mathrm{O}(^3P)$ at $E_{d3}=71\,600\pm400$ cm^{-1}, all lying below the first ionization potential [IP(0)

$=74\,721.7\ \mathrm{cm}^{-1}$ (Refs. 3 and 4)]. According to Miescher's pioneering work,[49] predissociation is fast for the np series, with the $l=1$ Rydberg electron interacting strongly with the $2p\sigma_u^*$ electron of the $A'\,^2\Sigma_u^+$ repulsive valence state. Accordingly, the decay width parameter $\Gamma_0(l)$ for the $np(l=1)$ series is expected to exceed those for the $ns(l=0)$ and $nd(l=2)$ series. Quantitative information on the decay width parameter for np $(N^+=0)$ series was obtained from the lifetimes of the $n=60-110$ states[10] analyzed according to the n^3 scaling law, Eq. (1.2), resulting in $\Gamma_0(p)=1610\ \mathrm{cm}^{-1}$ $(\pm 300\ \mathrm{cm}^{-1})$. Thus $\Gamma_0(p)$ is large, as expected.[49] The analysis (Table I) of the lifetimes of the $nf(N^+=2)$ $(n=40-60)$ series,[10] according to the n^3 scaling law, results in $\Gamma_0(f)=43\pm 8\ \mathrm{cm}^{-1}$, the low value of this width parameter is compatible with the characteristics of the nearly nonpenetrating f orbitals. Some information on the $\Gamma_0(s)$ and $\Gamma_0(d)$ decay widths can be inferred from the n dependence of the $np(N^+=0)$ series $(n=50-120)$ in sufficiently strong electric fields which allow for complete l mixing. Under the conditions of strong mixing, i.e., $F(n,l=1)>3$, one expects that the lifetimes $\langle\tau_{\mathrm{SM}}\rangle$ in this strong mixing domain are[39,40,45,46]

$$\langle\tau_{\mathrm{SM}}\rangle=n^4\hbar/\Gamma_0^T \tag{3.1}$$

with the $\langle\tau_{\mathrm{SM}}\rangle\propto n^4$ dependence being predicted by Chupka[45,46] and experimentally observed by Vrakking and Lee[10] for the strongly mixed np series. The numerical value of the decay width constant Γ_0^T in Eq. (3.1) is given according to the diagonal sum rule for the effective Hamiltonian by the sum of all the contributing doorway and escape states.[39,40] For the strongly mixed $np(N^+=0)$ series we have

$$\Gamma_0^T=\sum_l \Gamma_0(l). \tag{3.2}$$

The experimental data of Vrakking and Lee[10] for the strong mixing n^4 dependence results in $\Gamma_0^T=3200\ \mathrm{cm}^{-1}$ (± 500). As $\Gamma_0^T=\Gamma_0(s)+\Gamma_0(p)+\Gamma_0(d)+\Gamma_0(f)$ we utilize the $\Gamma_0(p)$ and $\Gamma_0(f)$ data estimated above and obtain $\Gamma_0(s)+\Gamma_0(d)\simeq 1500\ \mathrm{cm}^{-1}$. The individual s and d series decay width constants cannot be estimated and we have taken arbitrarily $\Gamma_0(s)=500\ \mathrm{cm}^{-1}$ and $\Gamma_0(d)=1000\ \mathrm{cm}^{-1}$. In Table II we summarize the input data for handling the predissociation dynamics of NO.

C. Predissociation dynamics for the Rydberg manifolds excited via the $nf(N^+=2)$ doorway state

The $nf(N^+=2)$ doorway state for a given n is $l=3$, $N^+=2, N=1$, and $M_N=0,\pm 1$ and we shall take its $M_N=0$ component. We construct now the effective Hamiltonian, Eq. (2.20), with Stark coupling between states with $N^+=2$. We shall represent the molecular states for $N^+=2$ by $|l,N\rangle$, where $N=l-2,l-1,l,l+1,l+2$ (for $l>1$). In view of the selection rules, Eq. (2.16), the effective Hamiltonian matrix couples two groups of $|l,N\rangle$ states, the coupling scheme (Fig. 1) being

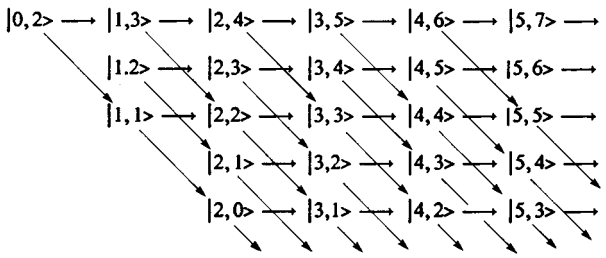

(3.3)

The electric field couples the first, third, and fifth rows in Eq. (3.3), resulting in the first group of $3n$-6 coupled states, which include the doorway state $|3,1\rangle$, and which will be used for the construction of the effective Hamiltonian. The second and the fourth rows in Eq. (3.3) are also coupled, forming the second group of $2n$-3 states. The Stark couplings, Eq. (2.7), subjected to the selection rules (2.16) are given by Eqs. (2.14) and (2.15) with the radial matrix elements being calculated from Eq. (2.17). The effective Hamiltonian has the schematic structure

$$\begin{array}{ccccccccccc}
[0,2] & V_2^0(0) & V_2^2(0) & 0 & 0 & 0 & 0 & 0 & 0 & \cdots \\
V_2^0(0) & [1,1] & 0 & V_0^{-2}(1) & V_0^0(1) & 0 & 0 & 0 & 0 & \cdots \\
V_2^2(0) & 0 & [1,3] & 0 & V_2^0(1) & V_2^2(1) & 0 & 0 & 0 & \cdots \\
0 & V_0^{-2}(1) & 0 & [2,0] & 0 & 0 & V_{-2}^{-2}(2) & 0 & 0 & \cdots \\
0 & V_0^0(1) & V_1^0(1) & 0 & [2,2] & 0 & V_0^{-2}(2) & V_0^0(2) & 0 & \cdots \\
0 & 0 & V_2^2(1) & 0 & 0 & [2,4] & 0 & V_2^0(2) & V_2^2(2) & \cdots \\
0 & 0 & 0 & V_{-2}^{-2}(2) & V_0^{-2}(2) & 0 & [3,1] & 0 & 0 & \cdots \\
0 & 0 & 0 & 0 & V_0^0(2) & V_2^0(2) & 0 & [3,3] & 0 & \cdots \\
0 & 0 & 0 & 0 & 0 & V_2^2(2) & 0 & 0 & [3,5] & \cdots \\
\vdots & \vdots & \vdots & \vdots & \vdots & \vdots & \vdots & \vdots & \vdots & \ddots
\end{array} \tag{3.4}$$

where the diagonal elements $[l,N]$ denote the energies of the $|l,N\rangle$ unperturbed states. The off diagonal elements $V(l)$ are proportional to the external electric field, and have the following general structures:

$$V_{-2}^{-2}(l)=e\langle \nu,l+1|r|\nu,l\rangle\left[\frac{(l-1)(l+1)}{(2l+1)(2l-1)}\right]^{1/2}F,$$

$$V_{0}^{-2}(l)=e\langle \nu,l+1|r|\nu,l\rangle\left[\frac{6}{(2l+1)(2l-1)(2l+3)}\right]^{1/2}F,$$

$$V_{0}^{0}(l)=e\langle \nu,l+1|r|\nu,l\rangle\left[\frac{l(l+2)(2l-1)(2l+5)}{(2l+1)(2l+3)}\right]^{1/2}F, \tag{3.5}$$

$$V_{2}^{0}(l)=e\langle \nu,l+1|r|\nu,l\rangle\left[\frac{6}{(2l+1)(2l+3)(2l+5)}\right]^{1/2}F,$$

$$V_{2}^{2}(l)=e\langle \nu,l+1|r|\nu,l\rangle\left[\frac{(l+3)(l+1)}{(2l+3)(2l+5)}\right]^{1/2}F,$$

with the radial matrix elements being given by Eq. (2.17). $\mathscr{H}_{\rm eff}$ for each n contains a single doorway state $|3,1\rangle$, reached by one-photon excitation from the intermediate state $A\ ^2\Sigma^+(N_A=0,J_A=1/2)$. There are nine $|l,N\rangle$ escape states, corresponding to the states with $l\leqslant 3$ in the effective Hamiltonian (3.4).

Typical results for the lifetime spectra and for the accessibility spectra for the $51f$ $(N^+=2)$ manifold at several electric field strengths ($F=0.05$–0.3 V/cm) are displayed in Fig. 3. Both the lifetimes spectra and the accessibility spectra reveal three branches which manifest the coupling within the $3n$-6 dimensional effective Hamiltonian, while the couplings between the different columns is weak, as compared with the intraline coupling in Eq. (3.3). In view of the low value of $\delta(f)$ (Table II) the onset of effective mixing of the $51f$ $(N^+=2)$ doorway state is realized at relatively low values of F, i.e., the reduced field, Eq. (1.4), assumes the value of $F(51,3)=1$ for $F=0.1$ V/cm. In this low F domain [Fig. 3(a)] there are three short lifetimes with substantial amplitudes [Fig. 3(d)]. With increasing F to the range >0.15 V/cm ($F>1.5$) the $f-|L\rangle$ mixing becomes more extensive with several (>3) short lived mixed states with appreciable amplitudes [Fig. 3(f)]. Approaching strong mixing for $F=0.3$ V/cm [$F(51,3)=3$] the lifetimes become more uniform [Fig. 3(c)], although there still exist some long-lived states with finite amplitudes. Of interest is the appearance of finite accessibility amplitudes at the high energy edge, i.e., $E\simeq 0.085$ $\rm cm^{-1}$ for $n=51$ [Figs. 3(e)–3(f)], which originate from nf–nd mixing. With increasing $F\geqslant 0.1$ V/cm the mixing of the f and the d escape states becomes extensive, being manifested by the appearance of a new branch around 0.095 eV in the accessibility and lifetime spectra [Figs. 3(d)–3(f)]. The high experimental spectral resolution (marked on Fig. 3) employed in the experimental study of the time-resolved and energy-resolved spectra[10] allows for a theoretical interrogation of the spectra and of the (average) lifetimes under narrow band excitation conditions.

In Fig. 4 we present our theoretical results for the energy-resolved PFI line shapes, Eq. (2.30), calculated for several F values in the range 0.03–0.3 V/cm. These spectra demonstrate (i) the appearance of a satellite or shoulder around $E\simeq 0$ (Fig. 4) which manifests field induced nf–$nl(l>3)$ mixing, starting at the lowest value of $F(=0.03$ V/cm). (ii) The appearance of an additional peak (the d band) around $E=0.085$ $\rm cm^{-1}$ (Fig. 4), which manifests nd–nf–$nl(>3)$ mixing. The onset of the nf–nd mixing is exhibited at $F=0.1$ V/cm, with the mixing of the nf doorway (and escape) state with the nd escape state becoming prominent with increasing F toward $F=0.3$ V/cm. We also confront the calculated spectra (Fig. 4) with the experimental spectra[10] (reproduced in Fig. 5). The experimental spectra[10] were reported at the external fields XF=0–0.237 V/cm, so that the effective field is $F=\mathrm{XF}+F_0$, where F_0 is the residual stray field. The overall agreement between theory and experiment[10] (Fig. 4 and insert in Fig. 5) seems to be reasonable provided that we choose $F_0\sim 0.05$ V/cm. To provide a more detailed comparison we consider the calculated and the experimental data for the areas of the spectral bands for the main peak due to doorway state and several effectively mixed states (labeled M) and of the satellite band at higher energies due to the $f-|L\rangle$ mixing (labeled L). The plots of the theoretical and the experimental values of the area ratios L/M (Fig. 5) nearly coincide for $F_0=0.06$ V/cm, providing an estimate of F_0. The appearance of the d peak at higher energies due to nf–nd field-induced mixing in the experimental spectrum (insert in Fig. 5), which is split from the main peak $\delta E(d-f)=0.12$ $\rm cm^{-1}$,[10] is in reasonable agreement with the value calculated from the respective quantum defects of $\delta E(d-f)=0.10$ $\rm cm^{-1}$. The experimental onset of the d peak (Fig. 4) is exhibited at XF=0.042 V/cm which together with the calculated onset implies that $F_0=0.06$ V/cm. The ratio d/M of the calculated and experimental[10] areas of the d band and of the main band (M) (Fig. 5) are consistent again with $F_0=0.06$ V/cm.

In the context of our lineshape analysis, we would like to point out that the lifetime spectra (Fig. 3) predict that the lifetimes at a constant value of F, under narrow band excitation conditions, will exhibit: (i) A gradual increase from the main peak towards higher energies, manifesting the $f-|L\rangle$ dilution at all values of F. (ii) When d mixing sets in ($F\geqslant 0.1$ V/cm) a modest decrease of the lifetimes at the high energy edge of the diluted $|L\rangle$ manifold will also be exhibited, due to $|L\rangle-|d\rangle$ mixing via sequential $d-f-|L\rangle$ coupling. (iii) The appearance of short lifetimes in the d band, which are determined by the relative fast decay of the mixed $d-f$ states. In view of the uncertainty in the value of $\Gamma_0(d)$ (Table II) prediction (iii) is only semiquantitative, as we expect that $\Gamma_0(d)\gg\Gamma_0(f)$. The predicted variation of the lifetimes across the PFI line shapes is of considerable interest and should be subjected to an experimental scrutiny. At present, experimental data for the decay times under narrow band excitation conditions are available only at the peak of the main band.[10]

We proceed to consider time-resolved information. The electric field dependence of the temporal population $P(t)$,

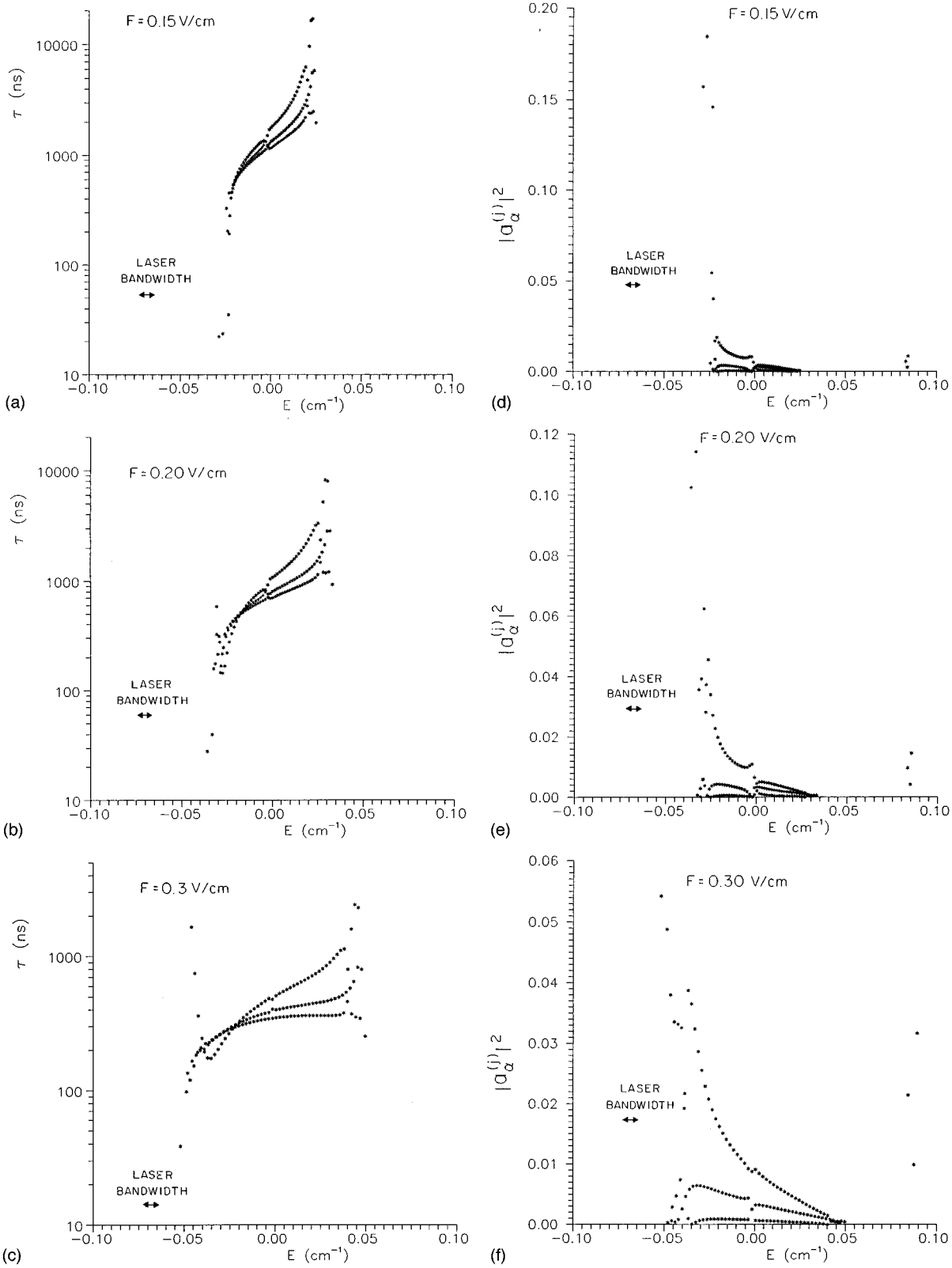

FIG. 3. The lifetime and accessibility spectra of the $n=51(N^+=2)$ Rydberg manifold with the $51f(N^+=2)$ doorway state. The spectral resolution is marked. (a) τ_j vs E_j for $F=0.15$ V/cm ($F=1.5$). (b) τ_j vs E_j for $F=0.20$ V/cm ($F=2$). (c) τ_j vs E_j for $F=0.30$ V/cm ($F=3$). (d) $|a_\alpha^j|^2$ vs E_j for $F=0.15$ V/cm ($F=1.5$). (e) $|a_j^\alpha|^2$ vs E_j for $F=0.20$ V/cm ($F=2$). (f) $|a_j^\alpha|^2$ vs E_j for $F=0.30$ V/cm ($F=3$).

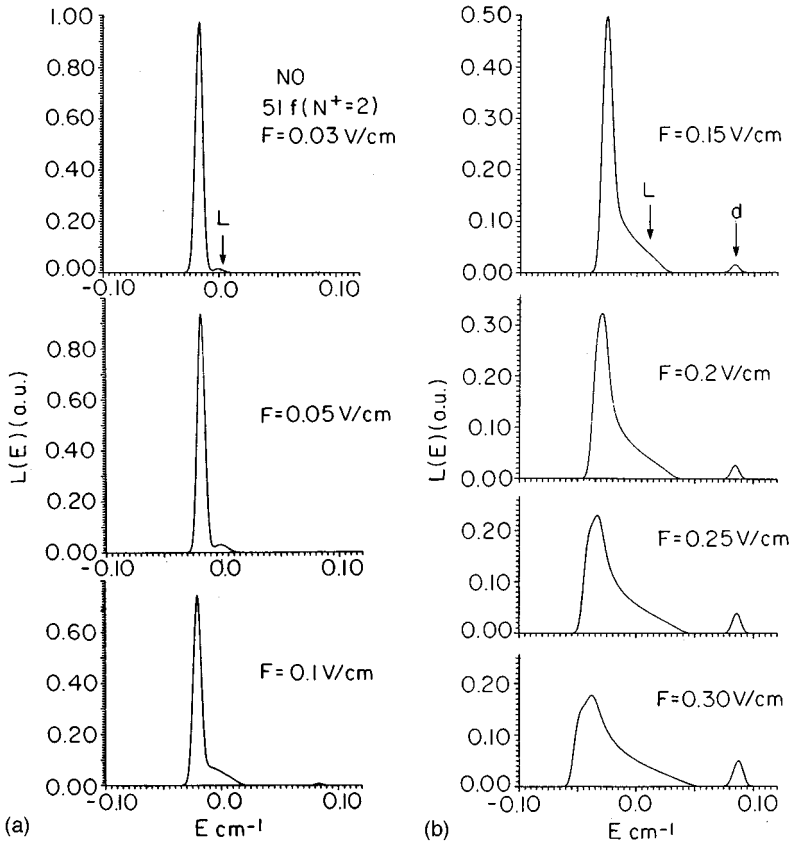

FIG. 4. Calculated energy-resolved PFI line shapes of the $51f(N^+=2)$ state at different strengths of the electric field (marked on the figures). Calculations of line shapes were performed using Eq. (2.30) and Eq. (2.27) with $\Delta\omega_p=5\times10^{-3}$ cm^{-1}. L marks the satellite band due to the $nf-nl(>3)$ mixing, while d marks the nd excitation. (a) $F=0.03$, 0.05, and 0.1 V/cm. (b) $F=0.15$, 0.2, 0.25, and 0.30 V/cm.

Eq. (2.25), under narrow band excitation, provides novel information on l mixing. The interrogation of $P(t)$ for narrow band excitation conditions in the vicinity of the maximum of $L(E)$ monitors the field-induced mixing in the energetic vicinity of the doorway state. We have used lifetime and accessibility data to construct $P(t)$ resulting from narrow band excitation ($\Delta\omega_p=8\times10^{-3}$ cm^{-1}) at the maximum of the $L(E)$ band (Fig. 4), spanning the dynamics of 3–5 mixed states, including the residue of the doorway state. The value of $\Delta\omega_p=8\times10^{-3}$ cm^{-1} used in the calculations somewhat exceeds the experimental spectral resolution[10] $\Delta\omega_p=5\times10^{-3}$ cm^{-1}, to avoid fluctuations in the calculated $P(t)$ and lifetime data (due to a small number of mixed states within $\Delta\omega_p$), which are averaged out in the experiment. In Fig. 6(a) we present the calculated time-evolution of $P(t)$ for the decay of the $51f(N^+=2)$ manifold at $F=0.01-0.30$ V/cm [$F(51,3)=1-3$] under narrow band excitation conditions. The time-resolved decay curves are nonexponential. At lower values of F (<0.20 V/cm) a weak long-time tail is exhibited, manifesting the contribution of the diluted $|L\rangle$ manifold. At higher values of F (>0.20 V/cm) the decay becomes nearly exponential due to effective field mixing. The characteristic (average) lifetimes, τ, for the decay of $P(t)$ are defined by

$$P(\tau)/P(0)=1/e. \tag{3.6}$$

The electric field dependence of the lifetimes of the narrow band excited $51f(N^+=2)$ manifold (Fig. 7) reveals a moderate stepwise increase [in the range $F=0.13-0.17$ V/cm, i.e., $F(51,f)=1.3-1.7$], which reflects effective mixing of the doorway state with the $|L\rangle$ states close to it. In Fig. 8 we

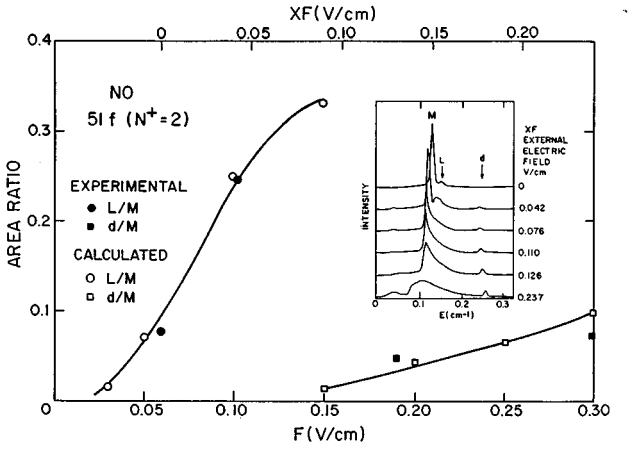

FIG. 5. Experimental and calculated data for the ratios L/M and d/M of the areas of the spectral bands for the main band (M), the effectively mixed ($l>3$) states (L) and the $l=2$ excitation (d). The experimental external electric field is XF, while the total electric field used in the calculations is F with $F=$XF$+0.06$ V/cm. The labeling of data is marked on the figure. The solid lines were drawn convecting the calculated data to guide the eye. The insert shows the experimental lineshape data of Vrakking and Lee (Ref. 10), which were used to calculate the area ratios.

compare the experimental results[10] for the lifetimes under narrow band excitation (obtained for an external field XF $=0-0.16$ V/cm with our calculated lifetime date. The overall agreement is satisfactory provided that we set again $F_0=0.06$ V/cm for the stray electric field (Fig. 8).

It is instructive to compare these data for narrow band excitation with the decay $P_{\mathrm{BB}}(t)$, Eq. (2.29), induced by broad band excitation and interrogation of the decay of the entire $51f(N^+=2)$ manifold [Fig. 6(b)]. $P_{\mathrm{BB}}(t)$ at lower ($F\leqslant 0.15$ V/cm) fields reveals a pronounced bimodal decay with long-time tails [range (A) in the terminology of Refs. 39 and 40], which marks the onset of effective coupling of the entire $|L\rangle$ manifold [Fig. 6(b)]. At higher fields ($F>0.15$ V/cm, i.e., $F>1.5$) effective mixing sets in, being manifested by a multiexponential slow decay [range (B)[39,40]]. The characteristics of the (broad band excited) $P_{\mathrm{BB}}(t)$ [Fig. 6(b)] qualitatively differ from those of the (narrow band excited) $P(t)$ [Fig. 6(a)], as the latter probes the entire level structure of the field mixed manifold, giving rise to long-time tails [range (A)]. The field-dependent lifetimes, Eq. (3.5), obtained for the $n=51(N^+=2)$ manifold under broad band conditions exhibit an onset which practically coincides with that for narrow band excitation (Fig. 7) with a much sharper rise in the range 0.13–0.15 V/cm ($F(51,f)=1.3-1.5$) (Fig. 7). The diluted higher field τ values ($F>0.17$ V/cm) are considerably larger under the broad band excitation conditions, i.e., $\tau(F=2)/\tau(F=0)=18$ for broad band excitation, while $\tau(F=2)/\tau(F=0)=4$ for narrow band excitation (Fig. 7). These quantitative differences mark the distinction between the dynamics of the mixed states in the energetic vicinity of the doorway state explored by narrow band excitation and those of the entire mixed manifold interrogated by broad band excitation. Finally, we note that for higher fields ($F=0.17-0.30$ V/cm, i.e., $F(51,f)=1.7-3.0$) the τ values under narrow band excitation moderately increase with increasing electric field, manifesting the enhancement of the dilution of the $51f$ doorway state and the states close to it with increasing F. In contrast, under broad band excitation τ decreases with increasing F in that range, exhibiting the enhanced mixing of the $51d$ (and p) escape states in the entire $51l(>3)$ manifold.

Complementary information is obtained from the time-resolved population $P(t)$ following narrow band excitation of the $51f(N^+=2)$ doorway state (for a fixed value of $F=0.04$ V/cm) over a range of $n=50-80$ values (Fig. 9). These time-resolved decay curves reveal a dramatic increase in the lifetimes in the vicinity of $n=63-68$ (Fig. 10), reflecting the effect of $51f-51l(l>3)$ mixing. The lifetime dependence on n reveals (i) the n^3 dependence for low $n(\leqslant 50)$, (ii) an abrupt increase in the range $n=63-68$ (Fig. 10) and (iii) a further increase in the range $m=70-80$. Range (i) is expected, while range (ii) manifests the (rather abrupt) onset of $51f-51l(>3)$ mixing. Range (iii) reveals almost complete l mixing which is expected to converge to a n^4 dependence of τ.[10,38,45–47] The comparison between the lifetimes obtained under narrow band and broad band excitation conditions (Fig. 10) reveals a similar trend for ranges (i) and (ii). The lifetimes in range (i) are invariant for the excitation conditions, while in range (ii) the increase of τ with increasing n exhibits a more abrupt rise for the broad band than for the narrow band excitation, reflecting the enhanced contribution of the mixed states energetically distant from the $51f$ doorway state. Regarding range (iii) we note that for large $n(>70)$ for $F=0.04$ V/cm, τ increases with increasing n for narrow band excitation, while under broad band excitation τ is practically independent of n in this range, reflecting the effect of the mixing of the $51d$ doorway state, which shortens the lifetimes. These distinct trends of narrow band and broad band excitation nicely reflect the properties of different domains of the mixed states, i.e., in the vicinity of the doorway state and the entire mixed n manifold, which we interrogated by these different excitation modes.

In Fig. 11 we confront the results of our theoretical calculations for narrow band excitation with the experimental

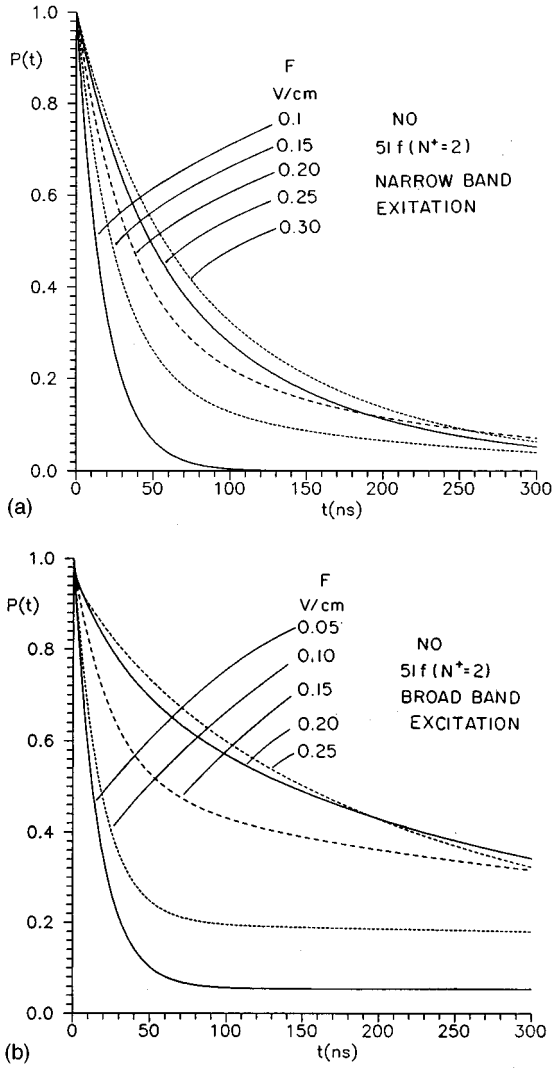

FIG. 6. Time-resolved population decay under different excitation conditions. The time-resolved population of the $n=51$ ($N^+=2$) manifold excited via the $51f(N^+=2)$ doorway state at several electric fields (marked on the figure). (a) Narrow band excitation ($\Delta\omega_p=8\times10^{-3}$ cm^{-1}) at the maximum of the PFI line shape (see the text). (b) Broad band excitation conditions, Eq. (2.29).

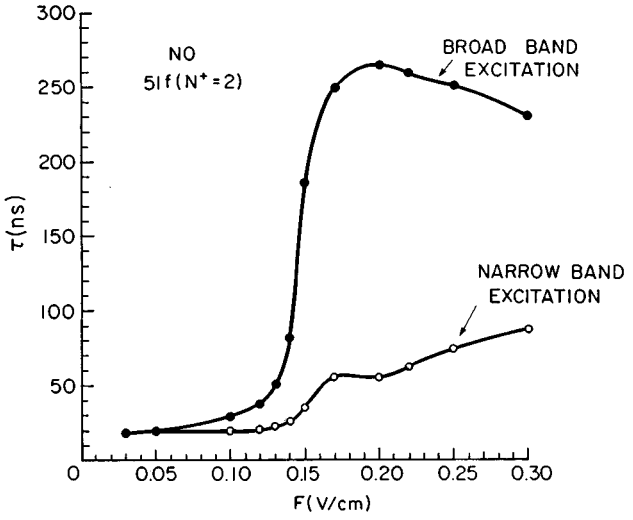

FIG. 7. The electric field dependence of the lifetimes τ [for e^{-1} decay of $P(t)$] of the $n=51$ ($N^+=2$) manifold excited via the $51f(N^+=2)$ doorway state, for narrow band excitation and for broad band excitation.

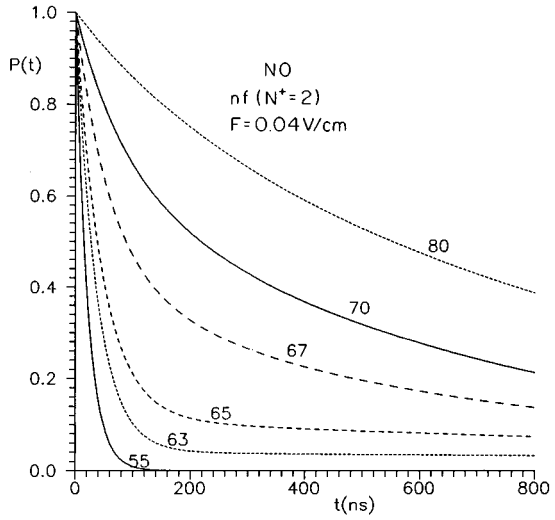

FIG. 9. The time-resolved population decay of $n=55-80$ ($N^+=2$) Rydberg manifolds, excited via the $nf(N^+=2)$ doorway state, with the n values marked on the curves. All data for narrow band excitation at $F=0.04$ V/cm.

results of Vrakking and Lee[10] for the n dependence of the lifetimes of the $nf(N^+=2)$ series experimentally obtained under minimum dc electric field conditions. The overall agreement between theory and experiment is reasonable for $F_0=0.04-0.05$ V/cm. Under these theoretical 'minimal electric field conditions' the dramatic experimental rise in τ with increasing n is well reproduced. Some deviations between the calculated and experimental lifetimes are exhibited at large values of $n(>70)$ where the experimental data show a very weak n dependence (and even an indication of a slight decrease of τ with increasing n), while our calculations for narrow band excitation conditions predict a moderate increase of τ with increasing n. The $n(<95)$ values considered herein are too low to warrant black body induced ionization effects.[82] It should be, however, borne in mind that the comparison between theoretical and experimental τ data for narrow band excitation require a more detailed characterization of the experimental narrow band excitation conditions. Further detailed experimental exploration of the energy dependence of τ under narrow band excitation conditions will be of interest.

Our theoretical analysis of the predissociation dynamics of the mixed $n(N^+=2)$ manifolds ($n=40-95$) with the $nf(N^+=2)$ doorway state for each n rests on the following assumptions:

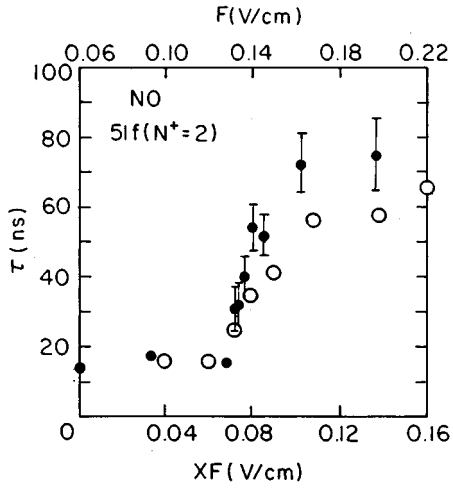

FIG. 8. A comparison between the experimental data (●) of Vrakking and Lee (Ref. 10) and our theoretical results (○) for the electric field dependence of the lifetimes of the $n=51$ ($N^+=2$) manifold excited via the $51f(N^+=2)$ doorway state under narrow band excitation conditions. The experimental external electric field is XF while the total electric field used in the calculations is F, with $F=\mathrm{XF}+0.06$ V/cm.

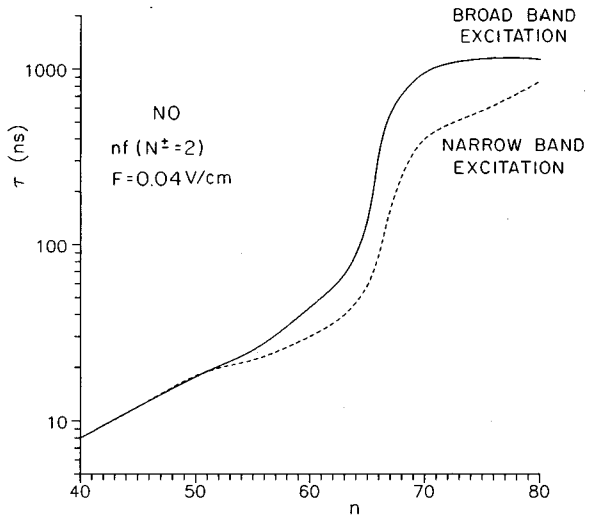

FIG. 10. The n dependence of the lifetimes τ of the $n=40-80$ ($N^+=2$) manifolds via the $nf(N^+=2)$ doorway states at $F=0.04$ V/cm. Narrow band excitation in the vicinity of the peak of $L(E)$ (dashed curve) and broad band excitation (solid curve).

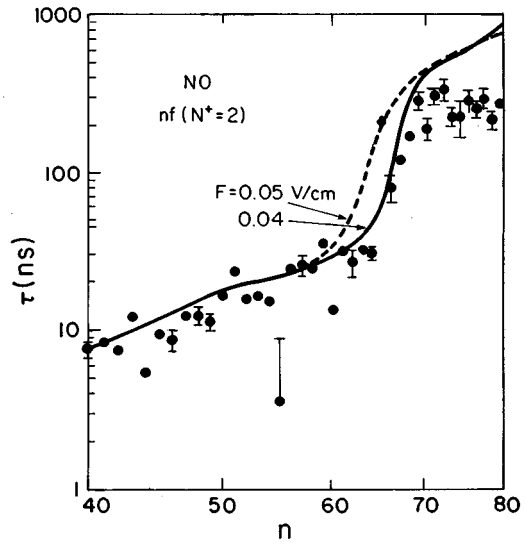

FIG. 11. A comparison of the results of the theoretical calculations for the n dependence of the lifetimes of the $n(N^+=2)$ manifolds excited by narrow band excitation via the $nf(N^+=2)$ doorway state (solid line $F=0.04$ V/cm, dashed line $F=0.05$ V/cm) with the experimental lifetimes (●) from Ref. 10.

(i) The dominance of the exterior electric field coupling, while intramolecular coupling effects are negligible (Sec. II C).

(ii) The construction of the effective Hamiltonian utilizing the available spectroscopic quantum defect $\delta(l)$ and decay widths parameters $\Gamma_0(l)$ data for lower n. In this context, the information of the decay width parameters of the nd states is incomplete.

(iii) The treatment of a single n manifold, which is justified for the n range of $n=40-95$.

(iv) With the nf doorway state, which is characterized by a low quantum defect (Table II), the relevant escape states involve only the nf and nd states in the relevant domain of electric fields, i.e., $F_0 \simeq 0.04-0.06$ V/cm for the stray field (Fig. 4) and $F \leqslant 0.2$ V/cm for the external field (Fig. 8). On the other hand, the mixing of the p and s states with a large value of their quantum defects is minor in this low range of F. Within our conceptual framework the treatment of the dynamics does not involve any auxiliary parameters, except the strength F_0 of the stray electric field. F_0 was determined to be in the range $F_0=0.04-0.06$ V/cm for the $nf(N^+=2)$ series from the line shape data in external fields for the $51f$ doorway state, from the external electric field dependence of the lifetimes for the $51f$ doorway states and from n dependences of the lifetimes in the stray field. Our value of F_0 is somewhat higher than the value $F_0=0.025$ V/cm estimated by Vrakking and Lee[10] in terms of the analysis of their experimental results by an equation of the form of Eq. (1.4), i.e., $Fn^5/\delta=$const, with a somewhat different numerical constant. As is evident from our rather lengthy analysis, a quantitative analysis of l mixing requires a detailed multichannel analysis.

D. Predissociation dynamics for the Rydberg manifolds excited via the $np(N^+=0)$ doorway state

The $np(N^+=0)$ doorway state for a given n manifold is $l=1$, $N^+=0$, $N=1$, $M_N=0$. There are $n|l,N\rangle$ $(N^+=0)$ states (for a given value of n) coupled by the Stark coupling, Eq. (2.7), with the selection rules, Eq. (2.16), the coupling scheme between the $|l,N\rangle$ states being

$$|0,0\rangle \rightarrow |1,1\rangle \rightarrow |2,2\rangle \rightarrow |3,3\rangle \rightarrow \cdots \rightarrow |m-1,n-1\rangle.$$

The doorway state is $|1,1\rangle$, while the escape states are $|0,0\rangle(s)$, $|2,2\rangle(d)$, $|3,3\rangle(f)$ and $|1,1\rangle(p)$. The large quantum defect of the np doorway state (Table II) implies effective mixing of all the escape states with $|L\rangle$. The effective Hamiltonian has the simple schematic structure

$$\begin{matrix} [0,0] & V_0^1 & \cdot & \cdot & \cdot & \cdot \\ V_0^1 & [1,1] & V_1^2 & & & \\ \cdot & V_0^2 & [2,2] & & & \\ \vdots & \vdots & & & & \end{matrix}, \tag{3.7}$$

where the off-diagonal matrix elements are obtained from Eqs. (2.14) and (2.15) with the radial integrals being given by Eq. (2.17). The effective Hamiltonian (Eq. 2.20), was constructed and diagonalized for $n=60-130$. For $n<100$ a single n manifold was used (Sec. II E). For $n \geqslant 100$ inter-manifold coupling sets in. The effective Hamiltonian for $n=100-130$ was constructed from three neighboring $(n-1)$, n, $(n+1)$ manifolds and the dynamics was calculated from the middle portion of the lifetimes and accessibility spectra. Narrow band excitation was performed with a width $\Delta\omega_p=8\times10^{-3}$ cm^{-1} in the vicinity of the residue of the doorway state, spanning 3–5 states.

In Fig. 12 we portray typical calculated data for the time evolution of the population $P(t)$ for $F=0.1$ V/cm over the range $n=110-135$. The time-resolved decay curves under narrow band excitation at a fixed value of $F=0.1$ V/cm (Fig. 11) reveal fast exponential decay at lower $n \leqslant 110$, with a marked retardation of the decay, i.e., the lengthening of the decay lifetimes in the range $n=115-130$. Of course, at lower fields, the n domain for the lengthening of the lifetimes moves towards higher values of n. In Fig. 13 we present the n dependence of the lifetimes calculated for several values of F (0.05–0.2 V/cm). At lower n the lifetimes exhibit the n^3 dependence, while the onset of the abrupt rise of the lifetimes with increasing n is exhibited at $n_M=115$ for $F=0.08$ V/cm, $n_M=110$ for $F=0.1$ V/cm, and $n_M=90$ for $F=0.2$ V/cm. The experimental results of Vrakking and Lee for the $np(N^+=0)$ series give, at the minimal residual electric field, $n_M=116$.[10] Accordingly, from our analysis of the dynamics of the $np(N^+=0)$ series we infer that $F_0=0.08$ V/cm. This value of $F_0=0.08$ V/cm is somewhat higher (i.e., by a numerical factor of 1.5–2.0) than the strength of the residual field $F_0=0.04-0.06$ V/cm extracted from the analysis of the dynamics of the $nf(N^+=2)$ series (Sec. III C). In any case, we conclude that our effective multichannel Hamiltonian provides a reasonable semiquantitative description of the dynamics of the Rydberg manifold of NO excited via the

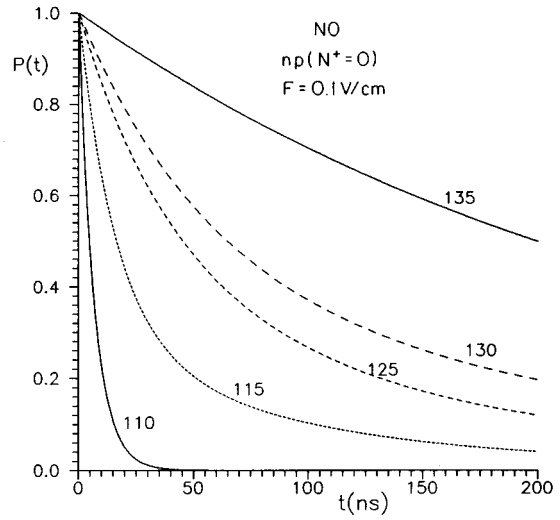

FIG. 12. The n dependence of the lifetimes τ of the $n=110-135$ $(N^+=0)$ manifolds excited via the $np(N^+=0)$ doorway state. Narrow band $(\Delta\omega_p=8\times10^{-3}\ \mathrm{cm}^{-1})$ excitation in the vicinity of the doorway state at $F=0.1$ V/cm.

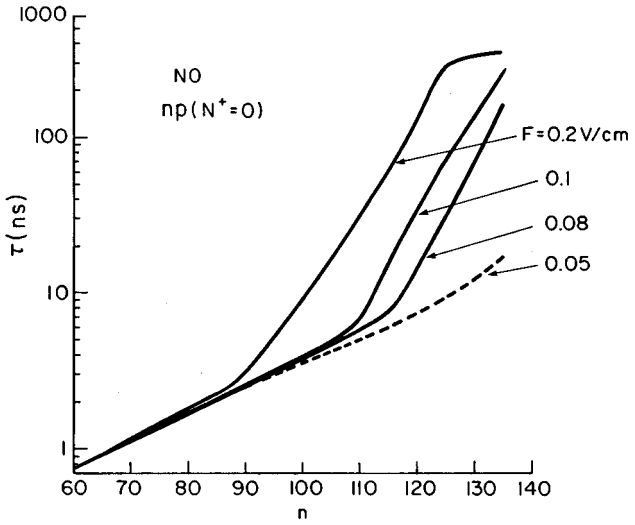

FIG. 13. The n dependence of the lifetimes τ of the $n=60-135$ $(N^+=0)$ Rydberg manifolds excited via the $np(N^+=0)$ doorway states at several electric fields $(F=0.05-0.2$ V/cm) marked on the curves.

$np(N^+=0)$ and the $nf(N^+=2)$ doorway states. The dominant coupling involves the exterior electric field coupling, while intramolecular Rydberg electron–core dipole coupling effects are, in general, negligible. Interesting exceptions to the rule of negligible intramolecular coupling are exhibited for some cases of accidental near-resonances, which will be now considered.

IV. NEAR-RESONANCES IN THE $np(N^+=0)$ RYDBERG SERIES OF NO

The $92p(N^+=0)$ and $95p(N^+=0)$ Rydbergs of NO, at a weak residual electric field $F_0\simeq0.04-0.08$ V/cm (Secs. III C and III D) exhibit abnormally long lifetimes.[10] These states are located well below the onset $n_M\simeq110$ for electric field induced mixing (Sec. III D). It was pointed out by Vrakking and Lee that the $92p(N^+=0)$ and the $95p(N^+=0)$ are nearly degenerate with the $80L$ $(l>3)(N^+=1)$ and the $82L$ $(l>3)(N^+=1)$ states, respectively, giving rise to possible rotational mixing effects.[10] In what follows we shall provide an analysis of these $np(N^+=0)$ near-resonances, which originate from sequential intramolecular $(H_{\mathrm{R\text{-}D}})$ and field induced (H_{STARK}) mixings. The realization of sequential mixing induced by $H_{\mathrm{R\text{-}D}}$ and by H_{STARK} requires fulfillment of the following energetic conditions. (i) The energy gap between $np(N^+=0)$ and $n'd(N^+=1)$ is small, being comparable to $\langle H_{\mathrm{R\text{-}D}}\rangle$. (ii) The energy gap between the $np(N^+=0)$ and the $n'L(N^+=1)(l>3)$ manifold is small, allowing for $n'd(N^+=1)-n'L(N^+=1)$ mixing via H_{STARK}.

The examination of the series $np(N^+=0)$, $nd(N^+=1)$ and nL $(l>3)(N^+=1)$ $(n=40-120)$ reveals only two near-resonances, which correspond to the

$$92p(N^+=0)\overset{H_{\mathrm{R\text{-}D}}}{\leftrightarrow}80d(N^+=1)\overset{H_{\mathrm{STARK}}}{\leftrightarrow}80L(N^+=1) \quad (4.1)$$

coupling and the

$$95p(N^+=0)\overset{H_{\mathrm{R\text{-}D}}}{\leftrightarrow}82d(N^+=1)\overset{H_{\mathrm{STARK}}}{\leftrightarrow}82L(N^+=1) \quad (4.2)$$

coupling, where $H_{\mathrm{R\text{-}D}}$ denotes the intramolecular Rydberg electron–core dipole coupling, Eq. (2.6), and H_{STARK} the exterior electric field coupling, Eq. (2.7). The energetics [with the energies being expressed relative to the first $(N^+=0)$ ionization potential] are

$$\begin{aligned} &E(92p(N^+=0))=-13.173\ \mathrm{cm}^{-1},\\ &E(80d(N^+=1))=-13.156\ \mathrm{cm}^{-1},\\ &E(80L(N^+=1))=-13.178\ \mathrm{cm}^{-1}, \end{aligned} \quad (4.3)$$

and

$$\begin{aligned} &E(95p(N^+=0))=-12.348\ \mathrm{cm}^{-1},\\ &E(82d(N^+=1))=-12.332\ \mathrm{cm}^{-1},\\ &E(82L(N^+=1))=-12.351\ \mathrm{cm}^{-1}. \end{aligned} \quad (4.4)$$

The coupling schemes (Fig. 14) involve mediated-sequential Rydberg–dipole $np(N^+=0)-n'd(N^+=1)$ coupling subjected to the selection rules $\Delta l=\pm1$ and $\Delta N^+=\pm1$, Eq. (2.10), and Stark $n'd(N^+=1)-n'f(N^+=1)-n'L(N^+=1)$ coupling subjected to the selection rules $\Delta l=\pm1$, $\Delta N^+=0$, Eq. (2.16). Alternatively, the coupling scheme (Fig. 14) can be described as mediated near-resonance coupling, where the intramolecular Rydberg–dipole coupling mediates the coupling of the $np(N^+=0)$ doorway state to the $n'd(N^+=1)-n'L(N^+=1)$ Stark manifold.

The intramolecular $H_{\mathrm{R\text{-}D}}$ interaction, Eq. (2.6), due to the dipole moment of NO^+, couples the $np(N^+=0)$ doorway state with the $nd(N^+=1)$ and the $ns(N^+=1)$ states. In the present case only the coupling with the $nd(N^+=1)$ state is

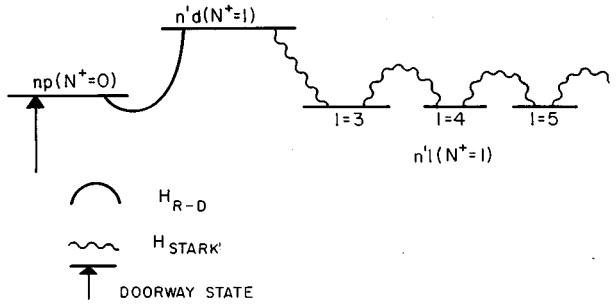

FIG. 14. A schematic description of the mediated-sequential coupling scheme $np(N^+=0) \overset{H_{R\text{-}D}}{\leftrightarrow} n'd(N+1) \overset{H_{STARK}}{\leftrightarrow} n'l(\geqslant 3)(N+1)$.

important because of its resonant condition. The intramolecular coupling matrix element is given by Eqs. (2.8) and (2.9), being expressed in the form

$$\langle np, N^+=0|H_{R\text{-}D}|n'd, N^+=1\rangle = -e\mu\langle \nu p|r^{-2}|\nu' d\rangle(\sqrt{2}/3), \tag{4.5}$$

with the radial matrix element being given by Eq. (2.11) with $\nu = n-\delta(p)$, $\nu' = n-\delta(d)$, $\lambda = 1-\delta(p)$ and $\lambda' = 2-\delta(d)$, with the quantum defects being given in Table II. The dipole moment of NO^+ was first calculated by Jungen and Lefebvre-Brion,[83] giving $\mu = 0.66 \pm 0.38$ D. Recent experiments and calculations of the dipole moment of the $A\ ^2\Sigma$ Rydberg state of NO resulted in $\mu = 1.1$ D.[84] We shall take the value of $\mu = 1.0$ D as a reasonable approximation for the dipole moment of NO^+. For the near-resonance interactions we shall utilize the approximate relation (see Sec. II C) given by Eq. (2.11) for the radial integral in Eq. (4.5) to obtain the following estimates for the strength of the intramolecular coupling:

$$\langle 92p, N^+=0|H_{R\text{-}D}|80d, N^+=1\rangle = -5.0\times 10^{-3}\ \text{cm}^{-1}$$

and

$$\langle 95p, N^+=0|H_{R\text{-}D}|82d, N^+=1\rangle = -4.6\times 10^{-3}\ \text{cm}^{-1}.$$

We note that these couplings are comparable to the corresponding energy gaps inferred from Eqs. (4.3) and (4.4). The experimental order of magnitude lengthening of the lifetimes of the $92p(N^+=0)$ and $95p(N^+=0)$ Rydbergs[10] cannot be attributed to near resonant coupling with the corresponding $n'd(N^+=1)$ state, and has to be supplemented by Stark coupling to the $n'L(N^+=1)$ manifold.

The matrix elements of the Stark Hamiltonian (Fig. 14) were calculated for electric field $F=0.04$ V/cm and $F=0.05$ V/cm (which is close to the stray field F_0) using Eqs. (2.13) and (2.14). The effective Hamiltonian (2.18) was constructed for the manifolds and coupling schemes (4.1) and (4.4) using the $\Gamma_0(l)$ data of Table II. The diagonalization of H_{eff} resulted in the following data for lifetimes (amplitudes) within an energy range of $\Delta E = 10^{-3}$ cm^{-1} around the doorway state:

(a) $92p(N^+=0)-80d(N^+=1)-80L(N^+=1)$ coupling; $F=0.05$ V/cm. A fast component 4 ns(0.618) and slow components 62 ns(0.039), 40 ns(0.060), and 47 ns(0.048).

(b) $95p(N^+=0)-80d(N^+=1)-80L(N^+=1)$ coupling; $F=0.04$ V/cm. A fast component 4 ns(0.67) and slow components 113 ns(0.021), 14 ns(0.034), 116 ns(0.023), and 58 ns(0.045).

Thus for the $92p(N^+=0)$ and $95p(N^+=0)$ Rydbergs slow components with a total amplitude of 0.4 are expected to be induced in a near-resonance effect (50–100 ns). These slow components appear in the narrow energy domain (10^{-3} cm^{-1}) in the vicinity of the doorway state, accounting for the lengthening of the lifetimes of these states. From this analysis we conclude that:

(i) Accidental resonances simultaneously coupled by intramolecular and Stark interactions result in mediated sequential l mixing. The sequential Stark coupling between the $|nlN^+\rangle$ doorway state and the $|n'l'(>3)N^{+\prime}\rangle$ manifold is mediated by intramolecular coupling with a $|n'l''N^{+\prime}\rangle$ mediating state.

(ii) The mediated-sequential Rydberg–core dipole and Stark couplings are subjected to strict selection rules.

(iii) The accidental near-resonances result in the breakdown of Hund's coupling case (d).

(iv) The accidental electronic near-degeneracy between the relevant Rydberg states bears an analogy to Fermi resonances for vibrational motion.

V. CONCLUDING REMARKS

From the analysis of the predissociation dynamics of NO high Rydbergs the following conclusions emerge:

(i) Origins of Rydberg dynamics. The dilution of Rydberg lifetimes should be attributed in most cases [see points (5) and (6) above] to l (or lm_l) electric field-induced coupling.

(ii) Unification. The analogy between intramolecular coupling, excitation and relaxation in a bound level structure of an isolated large molecule and the coupling, accessibility and decay of high Rydbergs in weak external fields establishes the unified description of radiationless transitions for intravalence excitations,[17–27] for low Rydbergs[85–87] and for very high Rydbergs.

(iii) Universality. Our analysis provides a universality principle for the description of the dynamics of high Rydbergs, involving predissociation and autoionization of diatomics, internal conversion of polyatomics and autoionization of atoms.

(iv) Quantification. Parameter-free multichannel calculations of the dynamics of electric field-induced l mixing for the autoionization dynamics of high atomic Rydbergs[40] and for the predissociation dynamics of the Rydbergs of NO presented herein, provide a satisfactory description of the experimental reality.[10,13]

(v) Extensions. An important issue is when does intramolecular Rydberg electron–core dipole coupling (or coupling with higher multipoles) become of importance in a

(below ionization) bound Rydberg level structure? Our analysis shows that for a diatomic molecule, i.e., NO intramolecular accidental resonances for low l ($\leqslant 3$) states can prevail, being subjected to strict selection rules. However, these near resonance effects are rare. Gilbert and Child[72] have demonstrated the spectroscopic effects of intramolecular coupling with a Rydberg quasicontinuum. In addition, in the presence of a weak ($F=0.05-0.1$ V/cm) electric field, intramolecular coupling between nearly degenerate pairs of states, in conjunction with Stark coupling, can induce l mixing via the mediated-sequential mechanism for a small number of doorway states.

(vi) l mixing cannot be induced by intramolecular coupling. Our analysis of the bottleneck effect (Sec. II C) demonstrates that intramolecular Rydberg electron–core dipole mixing and dynamics can prevail (for accidental near-resonances) only in the low l (<4) domain. l mixing via intramolecular coupling within the high inactive $|L\rangle(l\geqslant 4)$ manifold of nonpenetrating high n Rydbergs (with $n'\neq n$, in accord with the selection rule $\Delta N^+=\pm 1$ for dipole coupling) is precluded by the existence of large energy gaps and concurrently with vanishing dipole (and multipole) couplings. The bottleneck effect, which is general both for diatomics and for large molecules, implies that Rydberg dilution effects within the entire l manifold cannot be due to intramolecular Rydberg–core dipole (multipole) coupling and can be induced only by exterior electric field coupling. The intramolecular bottleneck effect advanced herein bears an analogy to previous discussion[88] and analysis[89,90] of large ΔN^+ changes in rotational autoionization in diatomics. In this context, Bordas *et al.*[88] pointed out that nonpenetrating high l Rydbergs are ineffective in $lN^+\rightarrow l'N^{+\prime}$ energy exchange, while Mahon *et al.*[89] and Merkt *et al.*[90] have shown that a series of sequential multipole interactions (via virtual mediating states) inhibit Rydberg electron–core rotation large angular momentum exchange, leading to the inevitable conclusion that electric field assisted coupling is essential.

ACKNOWLEDGMENTS

We are grateful to Richard Bersohn, Christian Jungen, Helene Lefebvre-Brion, and Marc J.J. Vrakking for illuminating discussions and for perceptive comments on the manuscript. We are grateful to Marc J.J. Vrakking for useful unpublished information. This research was supported by the Binational German–Israeli James Franck Program on Laser–Matter Interactions.

[1] K. Müller-Dethlefs, M. Sander, and E. W. Schlag, Chem. Phys. Lett. **112**, 291 (1984).
[2] K. Müller-Dethlefs, M. Sander, and E. W. Schlag, Z. Naturforsch. Teil A **39**, 1089 (1984).
[3] G. Reiser, W. Habenicht, K. Müller-Dethlefs, and E. W. Schlag, Chem. Phys. Lett. **152**, 119 (1988).
[4] K. Müller-Dethlefs and E. W. Schlag, Ann. Rev. Phys. Chem. **42**, 109 (1991).
[5] W. G. Scherzer, H. L. Selzler, E. W. Schlag, and R. D. Levine, Phys. Rev. Lett. **72**, 1435 (1994).
[6] W. G. Scherzer, H. L. Selzler, and E. W. Schlag, Z. Naturforsch. Teil A **48**, 1256 (1993).
[7] C. Alt, W. G. Scherzer, H. L. Selzle, and E. W. Schlag, Chem. Phys. Lett. **240**, 457 (1995).
[8] X. Zhang, J. M. Smith, and J. L. Knee, J. Chem. Phys. **99**, 3133 (1993).
[9] U. Even, R. D. Levine, and R. Bersohn, J. Phys. Chem. **98**, 3472 (1994).
[10] (a) M. J. J. Vrakking and Y. T. Lee, Phys. Rev. A **51**, R894 (1995); (b) M. J. J. Vrakking and Y. T. Lee, J. Chem. Phys. **102**, 8818 (1995).
[11] (a) I. Fischer, D. M. Villeneuve, M. J. J. Vrakking, and A. Stolow, J. Chem. Phys. **102**, 5566 (1995); (b) M. J. J. Vrakking, I. Fischer, D. M. Villeneuve, and A. Stolow, *Ibid*. **103**, 4538 (1995).
[12] F. Merkt, J. Chem. Phys. **100**, 2623 (1994).
[13] U. Even and M. Mühlpfort, J. Chem. Phys. **103**, 4427 (1995).
[14] F. Merkt, S. R. Mackenzie, and T. P. Softley, J. Chem. Phys. **103**, 4509 (1995).
[15] (a) U. Fano, Nuovo Cimento **12**, 156 (1935); (b) U. Fano, Phys. Rev. **124**, 1866 (1961).
[16] (a) H. Z. Buetler, Z. Phys. **86**, 710 (1933); (b) *ibid*. **93**, 177 (1935).
[17] M. Bixon and J. Jortner, J. Chem. Phys. **48**, 715 (1968).
[18] M. Bixon and J. Jortner, Mol. Cryst. **213**, 237 (1969).
[19] M. Bixon and J. Jortner, Isr. J. Chem. **1**, 189 (1969).
[20] M. Bixon and J. Jortner, J. Chem. Phys. **50**, 3284 (1969).
[21] M. Bixon and J. Jortner, J. Chem. Phys. **50**, 4061 (1969).
[22] M. Bixon, Y. Dothan, and J. Jortner, Mol. Phys. **17**, 109 (1969).
[23] S. Mukamel and J. Jortner, in *The World of Quantum Chemistry*, edited by R. Daudel and B. Pullman (Reidel, Dordrecht, 1974), pp. 145–209.
[24] S. Mukamel and J. Jortner, in *MTP International Review of Science*, edited by A. D. Buckingham and C. A. Coulson (Butterworth, London, 1976), Vol. 13, p. 327.
[25] S. Mukamel and J. Jortner, in *Excited States*, edited by C. E. Lim (Academic, New York, 1977), Vol. III, pp. 57–107.
[26] J. Kommandeur and J. Jortner, Chem. Phys. **28**, 273 (1978).
[27] R. D. Levine and J. Jortner, in *Advances in Chemical Physics*, edited by J. Jortner, R. D. Levine, and S. A. Rice (Wiley, New York, 1981), Vol. 47, pp. 1–114.
[28] U. Fano, Phys. Rev. A **2**, 353 (1970).
[29] U. Fano, J. Opt. Soc. Am. **65**, 979 (1975).
[30] H. Bethe and E. E. Salpeter, *Quantum Mechanics of One- and Two-Electron Atoms* (Springer, Berlin, 1957).
[31] R. S. Berry, J. Chem. Phys. **45**, 1228 (1966).
[32] N. Bradsley, Chem. Phys. Lett. **1**, 229 (1967).
[33] A. Russek, M. R. Patterson, and R. L. Becker, Phys. Rev. **167**, 167 (1967).
[34] R. S. Mulliken, J. Am. Chem. Soc. **91**, 4615 (1969).
[35] C. Jungen and D. Dill, J. Chem. Phys. **73**, 3338 (1980).
[36] G. Herzberg and C. Jungen, J. Mol. Spectrosc. **41**, 425 (1992).
[37] H. Lefebvre-Brion and R. W. Field, *Perturbations in the Spectra of Diatomic Molecules* (Academic, Orlando, 1986).
[38] J. Jortner and M. Bixon, J. Chem. Phys. **102**, 5636 (1995).
[39] M. Bixon and J. Jortner, J. Phys. Chem. **99**, 7466 (1995).
[40] M. Bixon and J. Jortner, J. Chem. Phys. **103**, 4431 (1995).
[41] D. Klar, K. Harth, J. Ganz, T. Kraft, M. W. Ruf, H. Hotop, V. Tsemekhman, and M. Ya. Amusia, Z. Phys. D **23**, 101 (1992).
[42] (a) K. Radler and J. Berkowitz, J. Chem. Phys. **70**, 216 (1979); (b) *ibid*. **70**, 221 (1979).
[43] J. Berkowitz, Adv. Chem. Phys. **58**, 1 (1988).
[44] C. Bordas, P. F. Brevet, M. Broyer, J. Chevaleyre, P. Labastie, and J. P. Perrot, Phys. Rev. Lett. **60**, 917 (1988).
[45] W. A. Chupka, J. Chem. Phys. **98**, 4520 (1993).
[46] W. A. Chupka, J. Chem. Phys. **99**, 5800 (1993).
[47] F. Merkt and R. N. Zare, J. Chem. Phys. **101**, 3495 (1994).
[48] E. Miescher, J. Mol. Spectrosc. **20**, 130 (1966).
[49] E. Miescher, Canad. J. Phys. **54**, 2074 (1976).
[50] E. Miescher and F. Alberti, J. Phys. Chem. **5**, 309 (1976).
[51] E. Miescher and K. P. Huber, *International Reviews of Science, Physical Chemistry* (Butterworth, London, 1976), Series 2, Vol. 3.
[52] P. C. Killpoar, G. E. Leroi, J. Berkowitz, and W. A. Chupka, J. Chem. Phys. **58**, 803 (1973).
[53] F. Alberti and A. E. Douglas, Can. J. Phys. **53**, 1179 (1975).
[54] E. Miescher, Y. T. Lee, and P. Gürtler, J. Chem. Phys. **68**, 2753 (1978).
[55] (a) K. Müller-Dethlefs, M. Sanders, and E. W. Schlag, Chem. Phys. Lett. **112**, 291 (1984); (b) Z. Naturforsch. Teil A **39**, 1089 (1984).
[56] Y. Anekazi, T. Ebata, N. Mikami, and M. Ito, Chem. Phys. **97**, 153 (1985).
[57] S. Fredin, D. Gauyacq, M. Horani, C. Jungen, G. Lefebvre, and F. Masnou-Seeuws, Mol. Phys. **60**, 825 (1987).

[58] D. T. Biernacki and S. D. Colson, J. Chem. Phys. **88**, 2099 (1988).
[59] K. Nakashima, H. Nakamura, Y. Achiba, and K. Kimura, J. Chem. Phys. **91**, 1603 (1989).
[60] D. Gauyacq, A. L. Roche, M. Seaver, S. D. Colson, and W. A. Chupka, Mol. Phys. **71**, 1311 (1990).
[61] (a) A. Fuji and N. Norita, J. Chem. Phys. **97**, 327 (1992); (b) Chem. Phys. Lett. **182**, 305 (1991); (c) J. Chem. Phys. **98**, 4581 (1993); (d) *ibid*. **103**, 6069 (1995).
[62] W. Kong, D. Rodgers, and J. W. Hepburn, J. Chem. Phys. **99**, 8571 (1993).
[63] S. T. Pratt, J. Chem. Phys. **98**, 9241 (1993).
[64] A. Nussenzweig and E. E. Eyler, J. Chem. Phys. **101**, 4617 (1994).
[65] (a) Ch. Jungen, J. Chem. Phys. **53**, 4168 (1970); (b) A. Giusti-Suzor and Ch. Jungen, *ibid*. **80**, 986 (1984).
[66] M. Raoult, J. Chem. Phys. **87**, 4736 (1987).
[67] K. Nakamura, H. Nakamura, Y. Achiba, and K. Kimura, J. Chem. Phys. **91**, 1603 (1989)
[68] J. T. Hougen, *The Calculation of Rotational Energy Levels and Rotational Line Intensities in Diatomic Molecules*, Natl. Bur. Stand. (U.S.), Monograph 115 (U.S. GPO, Washington, D.C., 1970).
[69] E. E. Eyler and F. M. Pipkin, Phys. Rev. A **27**, 2469 (1985).
[70] E. E. Eyler, Phys. Rev. A **34**, 2881 (1986).
[71] B. Ruscic and J. Berkowitz, J. Chem. Phys. **93**, 1747 (1990).
[72] R. D. Gilbert and M. S. Child, Chem. Phys. Lett. **187**, 153 (1991).
[73] (a) D. Bahat, U. Even, and R. D. Levine, J. Chem. Phys. **98**, 1744 (1993); (b) U. Even, M. Ben-Nun, and R. D. Levine, Chem. Phys. Lett. **210**, 416 (1993); (c) E. Rabani, L. Ya. Baranov, R. D. Levine, and U. Even, Chem. Phys. Lett. **221**, 473 (1994); (d) E. Rabani, R. D. Levine, A. Muhlpfordt, and U. Even, J. Chem. Phys. **102**, 1619 (1995).
[74] A. R. Edmonds, *Angular Momentum in Quantum Mechanics* (Princeton University, Princeton, 1974).
[75] G. Herzberg and Ch. Jungen, J. Chem. Phys. **84**, 1181 (1986).
[76] (a) U. Fano, Phys. Rev. A **2**, 353 (1970); (b) J. Opt. Soc. Am. **65**, 979 (1975).
[77] (a) S. Pasternack and M. Sternheimer, J. Math. Phys. **3**, 1280 (1962); (b) L. Armstrong, Phys. Rev. A **3**, 1546 (1971).
[78] T. Gallagher, *Rydberg Atoms* (Cambridge University, Cambridge, 1994), p. 348.
[79] J. K. G. Watson, Mol. Phys. **81**, 277 (1994).
[80] B. A. Zon, Sov. Phys. JETP **75**, 19 (1992).
[81] A. R. Edmonds, J. Picart, N. T. Minh, and R. Puller, J. Phys. B **12**, 2781 (1979).
[82] T. F. Gallagher, in *Rydberg States of Atoms and Molecules*, edited by R. F. Stebbings and F. B. Dunning (Cambridge University, Cambridge, 1983), p. 165.
[83] Ch. Jungen and H. Lefebvre-Brion, J. Mol. Spectrosc. **33**, 520 (1970).
[84] (a) J. A. Gray, R. L. Ferrow, J. L. Durant, and L. R. Thorne, J. Chem. Phys. **99**, 4327 (1993); (b) E. G. Glendening, D. Feller, K. A. Patterson, and R. J. Miller, *ibid*. **103**, 3517 (1995).
[85] (a) J. Jortner, J. Chim. Phys. Special Issue, *Transitions non Radiatives Dans Les Molécules*, 9 (1969); (b) J. Jortner and S. Leach, *ibid*. **77**, 7 (1980); (c) *ibid*. **77**, 43 (1980); (d) J. Jortner and G. C. Morris, J. Chem. Phys. **51**, 3689 (1969).
[86] R. L. Whetten, S. G. Grubb, C. E. Otis, A. C. Albrecht, and E. R. Grant, J. Chem. Phys. **82**, 1115 (1985).
[87] A. Amirav and J. Jortner, J. Chem. Phys. **82**, 4378 (1985).
[88] C. Bordas, P. Brevet, M. Boyer, J. Chevaleyre, and P. Lebastie, Europhys. Lett. **3**, 789 (1987).
[89] C. R. Mahon, G. R. Janik, and T. F. Gallagher, Phys. Rev. A **41**, 3746 (1990).
[90] F. Merkt, H. H. Fielding, and T. P. Softley, Chem. Phys. Lett. **202**, 153 (1993).